CHESAPEAKE ACOUSTIC RESEARCH INSTITUTE, LLC

TABLE OF CONTENTS

1 INTRODUCTION

Dr. Peter D'Antonio
President and Founder

The Chesapeake Acoustic Research Institute, LLC (CARI) was established in 2007 (www.cari-llc.com). Our mission is to provide acoustical exploration, experimentation and education to the architectural acoustics community to minimize unwanted noise, increase speech intelligibility and enhance music appreciation. In my careers in diffraction physics and acoustics, I have been privledged to know and collaborate with the brightest and most creative minds of my generation. I formed CARI, LLC as an acoustical think tank to take advantage of the unique expertise of these international colleagues and address difficult acoustical challenges. In effect, going beyond the NVLAP approach of just testing, by offering acousticial consultants an opportunity to collaborate with CARI acousticians to find solutions.

Exploration

CARI exlores innovative acoustical materials utilizing it's proprietary Shape Optimization software and other modeling tools, as well as innovative room designs to reduce noise, improve intelligibility and enhance music appreciation.

Experimentation

CARI is equipped to measure random and normal incidence absorption coefficients, as well as directional and random incidence scattering and diffusion coefficients, fabric transparency and flow resistivity.

Education

CARI offers acoustical education to corporate organizations, undergraduate and graduate acoustical programs and continuing education to the architectural and acoustical communities. In addition, Dr. D'Antonio provides thesis mentoring to acoustics students at international universities persuing Masters and Ph. D. degrees.

Currently, Dr. D'Antonio is providing seminars to undergraduates at the University of Hartford, University of Nebraska, University of Kansas, Rennselear Polytechnic Institute, Peabody Institute and the Cleveland Institute of Music. Dr. D'Antonio mentors Masters or Ph.D. research of students at RPI, ISVR, University of Nebraska, University of Sydney and Salford University.

Dr. D'Antonio also offers seminars on topics from the text "Acoustic Absorbers and Diffusers: Theory, Design and Application", by Dr. Trevor J. Cox and Dr. Peter D'Antonio, published by Taylor & Francis 2009 to all interested organizations, as well as seminars and workshops on the fundamentals of noise and vibration. Examples are provided for predicting noise isolation efficiency of floating floors/walls with software based on the Prognosis Method. Examples are also provided for predicting vibration isolation efficiency of machines, using software based on mobilities.

Biography

Dr. D'Antonio was born in Brooklyn, New York, in 1941. He received his B.S. degree from St. John's University in 1963 and his Ph.D. from the Polytechnic Institute of Brooklyn, in 1967. In 1974, he developed a widely used design for modern recording studios at Underground Sound, Largo, Maryland, utilizing a temporal reflection free zone and reflection phase grating diffusors. Dr. D'Antonio is founder and president of RPG Diffusor Systems, Inc., established in 1983. Dr. D'Antonio pioneered the sound diffusion industry and has significantly expanded the acoustical palette by creating and implementing a wide range of novel number-theoretic, fractal and optimized diffusing and absorbing surfaces, for which he holds many trademarks and patents. He has lectured extensively, published numerous scientific articles in technical journals and magazines and is the co-au-

Figure 1. Acoustic Absorbers and Diffusers: Theory, Design and Application. Top: 1st Edition Spon 2004. Bottom: 2nd Edition Taylor & Francis 2009.

thor with Prof. Trevor J. Cox at Salford University, of the reference book Acoustic Absorbers and Diffusers: Theory, Design and Application, Spon Press 2004 and 2nd Edition published by Taylor & Francis 2009. He served as Chairman of the AES Subcommittee on Acoustics Working Group SC-04-02, which published AES-4id-2001; is a member of the ISO/TC 43/SC 2/WG25 Working Group, which published ISO standard 17497-1:2004; and has served as adjunct professor of acoustics at the Cleveland Institute of Music, since 1991. He is a Fellow of the Acoustical Society of America and the Audio Engineering Society and a professional affiliate of the American Institute of Architects.

The quantifiable use of sound absorbing surfaces was initiated by Sabine over 100 years ago. CARI offers random incidence reverberation room absorption coefficient testing according to ISO 354 and normal incidence absorption absorption coefficient testing according to the two microphone method ISO 10534, down to 20 Hz. While several laboratories offer these established absorption testing services, standardized testing methodology for scattering surfaces is only recently been standardized by ISO. Since Dr. D'Antonio has played such a intimate role in developing these standards, we are especially qualified to provide testing services for both the scattering and diffusion coefficient.

The commercialization of sound diffusing surfaces occurred in 1983 by RPG Diffusor Systems, Inc. and hence the use of these surfaces is relatively new by comparison. Over the past three decades Dr. D'Antonio has collaborated with international acousticians in standards organizations to develop standards for measuring and characterizing sound scattering surfaces. The method proposed by Dr. D'Antonio was accepted by the AES Standards committee SC-04-02 and published as an AES Information Document, AES-4id-2001, JAES, Vol. 9(3), pp 148-165 (March 2001). This method is now standardized as ISO 17497-2. The goniometer boundary measurement procedure developed at RPG Diffusor Systems and incorporated in these standards is described below. In addition to the diffusion coefficient, Dr. D'Antonio has served on the of ISO/TC 43/SC 2 working group 25 to create the standard for the scattering coefficient, which was published as ISO 17497-1 and is also described below.

Since testing of scattering surfaces can be done in scale, as opposed to absorbing surfaces, CARI provides the capability to fabricate scaled samples using its rapid protoyping 3D printer.

Lastly, CARI has also developed a fabric transparency test, using its impedance tube, which is described below.

CARI is a unique research facility in that it also provides acoustical collaboration to interpret measurement data and possible approaches to improve performance.

2 COEFFICIENT SUITE

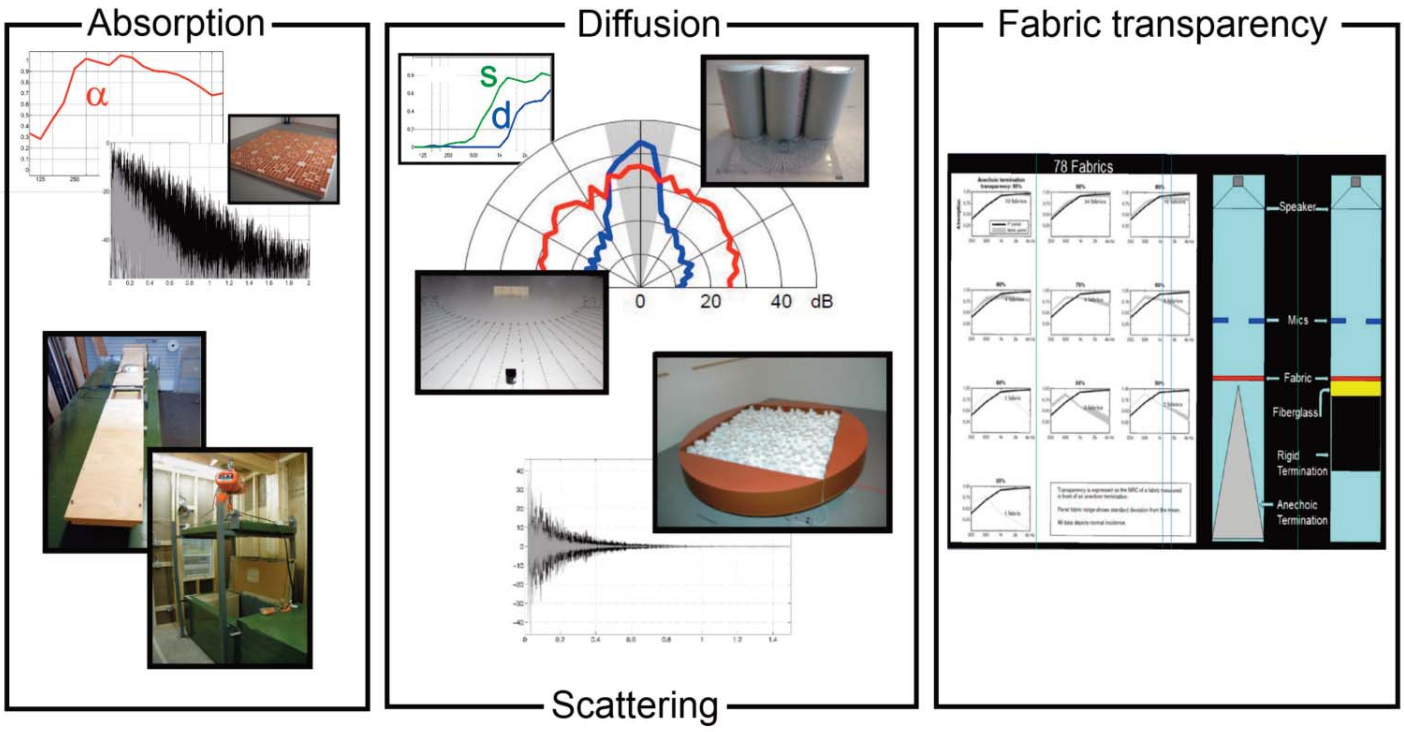

Figure 2.1 Measurement of the absorption coefficient, α, is carried out using the rev room, top of Absorption panel, or normal incidence using the impedance tube method, shown in the lower area of the Absorption panel. Measurement of scattering surfaces is depicted in the center panel showing Diffusion and Scattering methodology. The scattering coefficient, s, can be obtained by the rotating table method shown in the lower area and by cross correlation of the sample and reflector polar responses shown in the upper area obtained using the goniometer method which also is used to determine the diffusion coefficient, d.

CARI offers an extensive Coefficient Suite, Figure 2.1, with improved hardware and all new data collection and processing software. With respect to absorption, we can determine the random incidence absorption coefficient according to ISO 354 and the normal incidence absorption coefficient, according to ISO10534-2, as seen in the left Absorption panel in Figure 2.1.

Figure 2.2 Absorption Coefficient ISO 354: How much of the incident sound is absorbed (Must be measured full scale).

The quantifiable use of sound absorbing surfaces was initiated by Sabine over 100 years ago. The random incidence absorption coefficient is a measure of the amount of incident sound that is absorbed. It is not an intrinsic property of the material, because it is dependent on measurement conditions. It can be calculated and must be measured in full scale. It is determined according to ISO 354 and ASTM C423-90, Figure 2.2.

While several laboratories offer established absorption testing, the evaluation of scattering surfaces is only recently been standardized by ISO 17497-1 and ISO 17497-2, respectively.

Figure 2.3 Scattering Coefficient ISO 17497-1: How much of the incident sound is scattered away from the specular zone (Can be measured in scale and calculated).

The scattering coefficient, s, can be obtained in two ways. The ISO 17497-1, using the rotating table method, Figure 2.3 and bottom of center Scattering panel in Figure 2.1 and the correlation scattering coefficient, by cross correlating the polar responses for a scattering sample and a reference reflector, top of center Scattering panel in Figure 2.1.

The commercialization of sound diffusing surfaces occurred in 1983 by RPG Diffusor Systems, Inc. and hence the use of these surfaces is relatively new by comparison. Over the past two decades in-

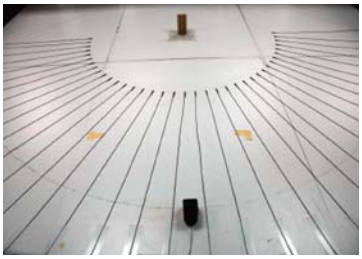

Figure 2.4 Diffusion Coefficient ISO 17497-2: How uniformly is the incident sound scattered (Can be measured in scale and calculated).

ternational acousticians have developed a standard for measuring and characterizing sound diffusing surfaces. The method proposed by D'Antonio was accepted by the AES Standards committee SC-04-02 and published as an AES Information Document, AES-4id-2001, JAES, Vol. 9(3), pp 148-165 (March 2001). This method is in the final stages of acceptance as ISO 17497-2. The goniometer boundary measurement procedure developed at RPG Diffusor Systems and incorporated in these standards is shown in Figure 2.4 and described in this brochure. The diffusion coefficient, d, is obtained according to ISO 17497-2, using 32 simultaneous impulse responses from a boundary plane goiniometer.

Since fabrics are extensively used to cover absorbers and scattering surfaces, we also offer Fabric Transparency tests, Figure 2.1 right panel. These tests include transfer function transparency testing evaluating application over a scattering surface and normal incidence absorption coefficient testing in the impedance tube to evaluate the effect of applying the fabric over a porous absorber.

3 ABSORPTION COEFFICIENT MEASUREMENT PROCEDURES

3.1 ISO 354 Random Incidence Absorption Coefficient Testing

The sound field at low frequencies in a room is determined by a small number of eigen-frequencies in a certain frequency band, eg. third-octaves. If this number is too small the condition of a diffuse sound field is not fulfilled. Therefore, the whole frequency range is split into three ranges wherein different measurement techniques are applied. At one-third octaves comprising more than 20 eigen-frequencies, the standardized ISO 354 measuring technique is used. In this case the source is mounted in a corner and the sample is places asymmetrically near the center of the room as described in the standard.

At one-third octaves with an eigen-frequency density between 5 and 20 the standardized method is modified. The excitation of the sound field as well as the measurement of the reverberation time with and without the test object are performed in the corners of the room where all eigen-frequencies in this frequency range are excited and can be registered. The absorption coefficient is calculated with the same formulas given in ISO 354.

At one-third octaves with 5 or less eigen-frequencies each eigen-frequency of the room is excited separately with a sine wave signal. The decay times at a particular eigen-frequency without and with the sample present in the room are measured. From these the effective absorption coefficient at this particular eigen-frequency of the room is calculated, using a modified formula for the mean free path.

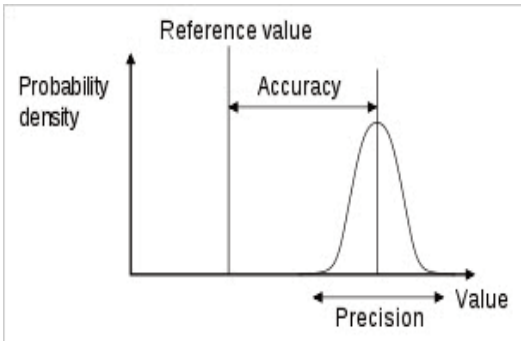

Figure 3.1 Comparison between precision and accuracy.

Let's begin by comparing precision and accuracy, because an important criterion for a standardized measurement is reproducible accuracy in many labs. Precision or reproducibility is the degree to which repeated measurements under unchanged conditions yield the same results. Accuracy of a measurement system is the degree of closeness of measurements of a quantity to its actual (true) value. One can make many precise measurements of the circumference of a circle, but if the mean does not equal pi times the diameter, the result is not accurate. At the moment the

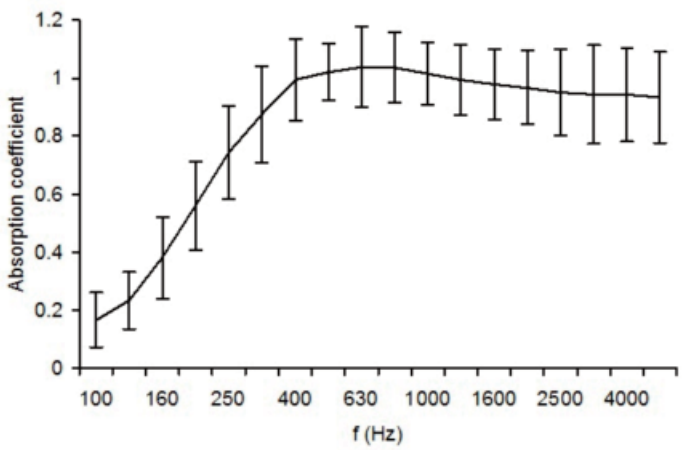

Figure 3.2. Comparison of measured absorption coefficients in 24 laboratories with 95% confidence limits.

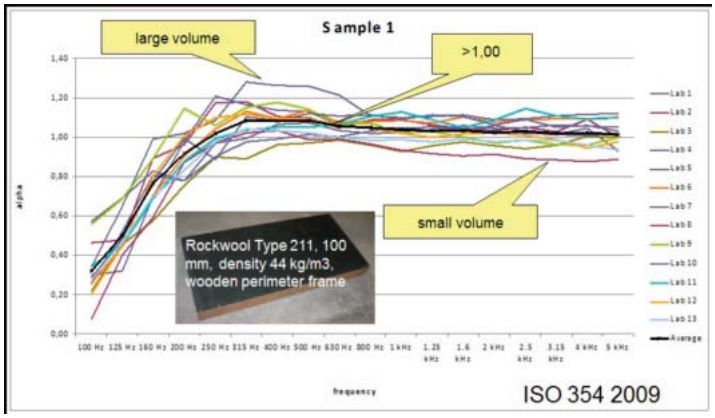

Figure 3.3. Round robin experiment involving 13 laboratories of various shape and volume, using a Rockwool Type 211, 100mm thick with a density of 44 kg/m3 surrounded by a wooden perimeter. The average date exceed 1.

random incidence absorption coefficient is neither accurate nor reproducible.

The random incidence absorption coefficient is a measure of the amount of incident sound that is attenuated
It is determined according to ISO 354/ASTM C423-09 in a reverberation chamber. Unfortunately, this coefficient is not a material property like flow resistivity or porosity, because it is influenced by mounting, sample size, edge effects and room diffusivity. It is a proof-of-performance metric and should be included in all CSI Specifications. It is used to comparatively evaluate absorbing surfaces and in computer models

After more than 100 years, we still do not know the actual random incidence absorption coefficient for an absorber and current standards are inadequate and under intense review! Comparison of measured absorption coefficients for a single sample in twenty four laboratories is shown in Figure 3.2. The mean absorption coefficient across all laboratories is shown, along with error bars indicating the 95% confidence limit in any one laboratory measurement. In an-

other round robin experiment by TC43/SC2/WG26 (reference) involving 13 laboratories of various sizes, geometry and volume a similar wide variation was found, as shown in Figure 3.3. This experiment was aimed at revising ISO 354 by considering the possible use of the Eyring equation, which is more accurate than Sabin for high absorption, the influence of suspended ceiling diffusers, which reduce the mean free path 4V/S, and is not accounted for in the Sabin equation, low frequency impedance discontinuity edge dif-

Figure 3.4. Top: Traditional suspended ceiling diffusers, which reduce mean free path and room volume in unpredictable ways. Bottom: Suggested boundary mounted diffusers allow accurate calculation of the room surface area and volume. Lautenback & Vercammen, Proc. 20th ICA 2010.

fraction and the use of possible reference materials. Other issues of concern in current rev room measurements include the diffusivity of the sound field and the uniformity of the incident sound intensity distribution, which is a function of room shape and dimensions, surface absorption, source and sample locations (Cheol-Ho Jeong, J. Acoust. Soc. Am., Volume 127, Issue 6, pp 3560-3568 (June 2010).

In Figure 3.4, we show two rev rooms by Lautenbach & Vercammen, Proc. 20th ICA, Sydney Australia (August 2010). One with the traditional suspended diffusers and another with proposed boundary diffusers. The suspended diffusers affect the volume in an undetermined way due to shadowing, whereas the use of known geometry diffusers allows accurate calculation of the room surface area and volume.

In Figure 3.5, it is illustrated how the mean free path is reduced with traditional suspended ceiling diffusers. It may be possible to determine the mean free path from a ray tracing program and use it to correct the room volume, thereby lowering the calculated absorption coefficient.

The familiar edge effect, which is related to the wavelength relative to the dimensions of the sample, was revisited by de Bruijn. The absorption of a finite sample is composed of the absorption of an infinite sample as and a factor b multiplies by the edge length E. Figure 3.6 shows b from experimental and theoretical studies. In Figure 3.7, we show a photo of the first rev room using boundary diffusers, following the current suggestions of ISO 354 working group.

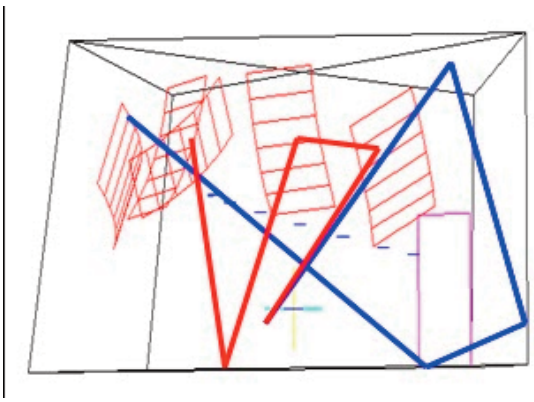

Figure 3.5. Ceiling clouds reduce the mean free path. Lautenback & Vercammen, Proc. 20th ICA 2010.

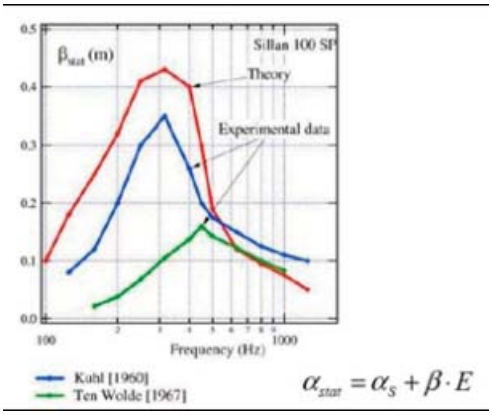

Figure 3.6. Graph shows beta from experimental and theoretical studies. A. de Bruijn, The edge effect of sound absorbing materials "revisited", NAG 2007 Y. Kawai and H. Meotoiwa, Acoust. Sci. & Tech. 26, 2 (2005).

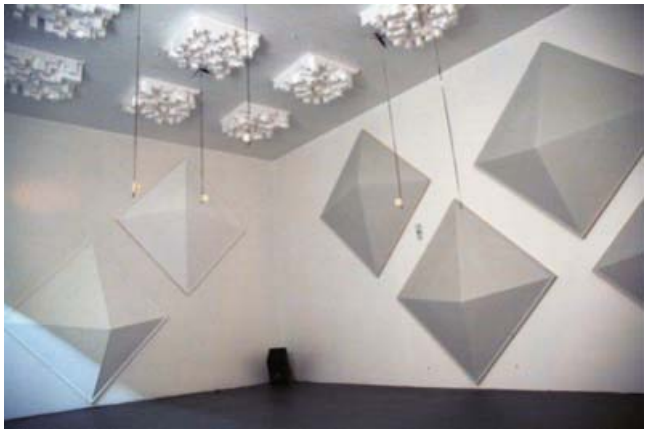

Figure 3.7. The first rev room using boundary diffusers, following the recommendations of the ISO 354 working group.

3.1.1 Data Processing

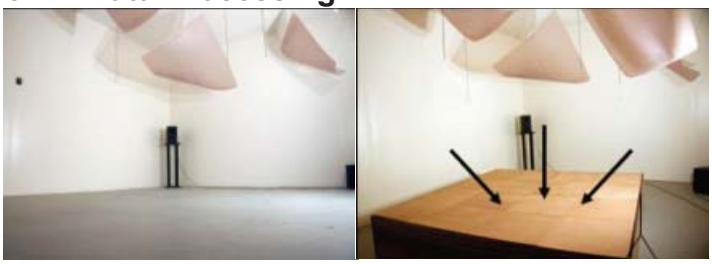

Figure 3.8. Top: Empty rev room showing diffusing clouds, loudspeaker and microphones. Bottom: Rev room with perforated wood panels in an E mount.

According to ISO 354, the reverberation time is determined with and without the sample present as shown in Figure 3.8. For the empty room and sample tests, a total of 6 impulse responses are measured, using a 131, 071 point MLS excitation of length of 2.73 seconds, with 4 averages and 1 pre-excitation. 6 fixed omnidirectional DPA microphones distributed throughout the room and two Paradigm Studio/20 reference speakers located in opposite corners are used. The MLS stimulus was generated with the EASERA software, sent to both speakers and the 6 impulse responses were recorded simultaneously, using a MOTU 8Pre. Data were processed according to ISO 354, using both Sabine, aS, and Eyring, aE. The air temperature and relative humidity conditions are monitored and recorded during the empty and full room measurements.

$$a_s = 55.3\frac{V}{S}\left(\frac{1}{c_2 T_2} - \frac{1}{c_1 T_1}\right) - \frac{4V}{S}(m_2 - m_1)$$

$$a_E = \frac{S_0}{S}\left(\exp\left(-\frac{V}{S_0}\left(\frac{55.3}{c_1 T_1} - 4m_1\right)\right) - \exp\left(-\frac{V}{S_0}\left(\frac{55.3}{c_2 T_2} - 4m_2\right)\right)\right)$$

where
m1 = air attenuation empty
m2 = air attenuation with sample
c1,2 = speed of sound
V = room volume
a = random-incidence absorption coefficient
S = sample surface area
S0 = room surface area

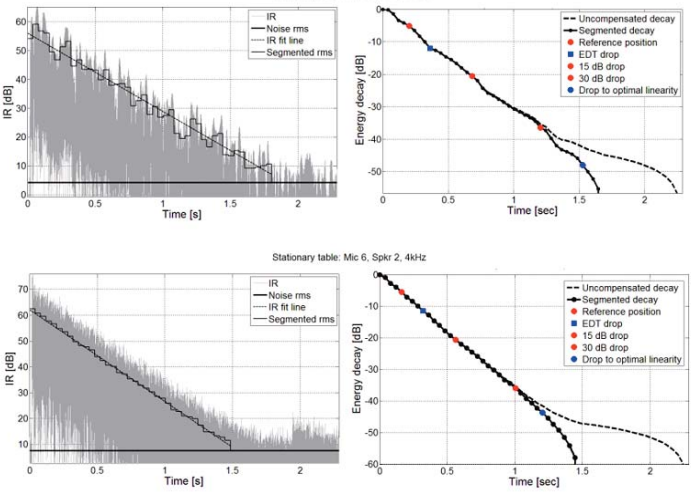

Figure 3.9 Top Left: Impulse response squared at 125 Hz. The energy decay is divided into segments and the RMS value determined (step function). A best fit line is determined from the highest correlation with the energy decay to find the optimal point in time where the line intersects the RMS noise to allow proper noise removal. Top Right: The backward integration of the segmented decay is shown with and without compensation for noise. The optimal linearity point (blue dot) cannot be determined without noise compensation. Points for -5dB reference position, EDT drop, 15 dB drop, 30 dB drop and optimal linearity drop. Using the optimal linearity drop is very important at low frequency where the segmented decay is non-linear. Dashed line is the uncompensated decay. Bottom Left: Impulse squared at 4 kHz. It can be seen that the segmented decay is very linear. Bottom Right: Even at this frequency noise compensation is still required to locate the time at which optimal linearity is achieved (blue dot). Dashed line is the uncompensated decay.

Sabine and Eyring converge at low absorption, but diverge when the absorption is high, in which case Eyring is more appropriate.

Because the measurement of the reverberation time from the slope of the Schroeder integration of the impulse response is so dependent on the extraction of noise, we de-

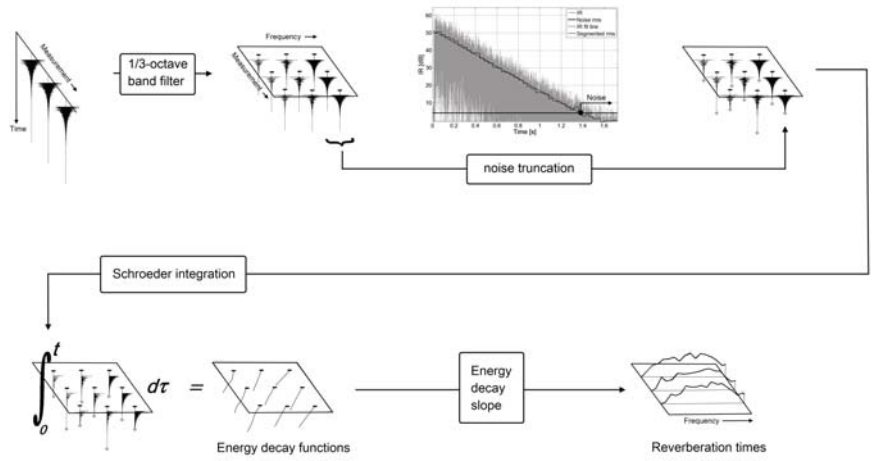

Figure 3.10 illustrates the data flow for reverberation time calculation. Broadband impulse response measurements are filtered into 1/3-octave bands. The matrix of filtered responses is then passed through a noise truncation algorithm. Exponentially decaying data is separated from the noise floor using root-mean-square values of short (40 ms) time segments. Energy decay associated with each impulse response is obtained via the Schroeder integral, and the slope of this decay yields reverberation time for each measurement as a function of frequency.

veloped an algorithm to optimally remove it. If noise is not properly removed you can incur a significant error, especially at low frequency where modal effects result in non-linear features in the backward integration.

The noise removal procedure is shown in Figure 3.9 at 125 Hz, where modal effects are present and at 4 kHz, where the Schroeder integration is more linear.

A schematic representation of the data reduction process from impulse response to reverberation time is shown in Figure 3.10.

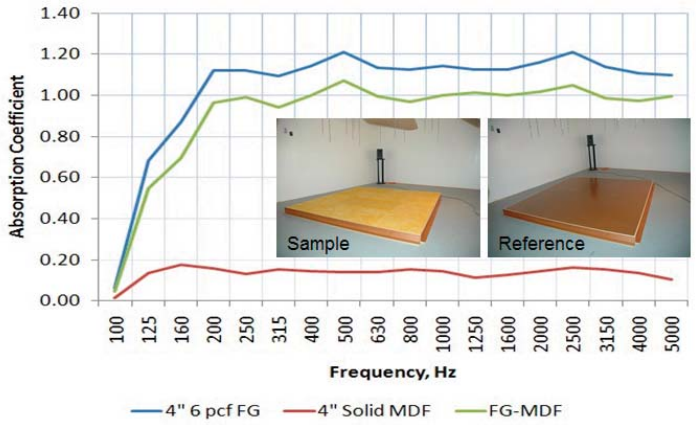

Figure 3.11. Calibrated absorption coefficient for a 4" fiberglass sample in an A mount on the chamber floor, using a non-diaphragmatic 4" MDF sample of the same area and perimeter as the fiberglass, as a reference reflector, processed using Eyring.

3.1.2 Calibration Using a Reference Reflector

To improve the reproducibility of the random incidence absorption coefficient among laboratories, it is is proposed that an additional measurement be added to ISO 354 for a reference reflector with the same height, area and perimeter as the absorptive sample under test. This reference reflector shall be fabricated from a material that has "zero" absorption. This could be multiple layers of MDF fully sealer, stainless steel, aluminum, plastic, etc. or any non-diaphragmatic, non-absorptive material. The non-absorptive reference will experience the same non-ideal reverberation chamber conditions as the absorptive sample, which may result in its absorption coefficient being greater than zero. This deviation from zero would be considered the error that the non-ideal chamber measurement introduces. To correct for this, it is proposed that the non-absorptive reference reverberation times be used as the reference instead of the empty room, as is the current situation. In addition, to this proposal it is also suggested that the Eyring formula be used instead of Sabine. This is necessary because, while Sabine may be appropriate for the non-absorptive reference measurement, it is not appropriate for the highly absorptive sample and substituting the non-absorptive reference for the empty room would not be accurate under these conditions.

This is really no different that what is currently being done in ISO 17497-1, in which the stationary and rotating table are used as references for the stationary and rotating samples under test.

An experiment was carried out in an experimental 75 m3 rev room, in which the absorption coefficient of a solid 4" (102 mm) MDF sample, with the same perimeter/area as a 4" thick, 6 pcf (96 kg/m3), fiberglass sample, was measured. The thesis being that this non-diaphragmatic MDF sample, which was fully sealed several times, would experience the same chamber deficiencies as the absorptive sample and hence be used to correct these errors. In this experiment the solid, non-diaphragmatic sample with the same perimeter/area as the absorptive sample under test is used as the reference, instead of the empty room.

In conclusion, the data illustrated in Figure 3.11 indicate that the reference non-absorptive reference reflector shows non-zero absorption. Since the reflector cannot absorb sound, this deviation from zero is used to correct the absorption coefficient of the absorptive sample. Because the absorptive sample offers significant absorption, Eyring was used to properly calculate this coefficient, using the MDF sample as reference, instead of the empty room. This correction results in lowering the absorption coefficient to oscillate about for all frequencies.

3.2 ISO 10534-2 Impedance Tube Testing

Figure 3.2.1 Impedance tubes: Left: 24"; Right 6.3"

Figure 3.2.1 shows the 24" (610 mm) and 6.3" (160 mm) square impedance tubes, providing normal incidence absorption coefficients from 20 - 4,000 Hz. The 610 mm tube has a bandwidth of 20 Hz - 200 Hz and the 160 mm tube provides a bandwidth of 63 Hz - 4000 Hz. For homogeneous samples the 160 mm tube provides an adequate bandwidth. However, for low frequency absorption measurements resonant systems, where the size is important, and non-homogeneous samples, where a sufficient represenation of the sample is necessary, the 610 mm tube is required. In certain cases both tubes can complement each other.

The standing wave tube enables both the normal incidence absorption coefficient and surface impedance to be measured. This is a very useful test method as it enables the absorption coefficient and impedance to be measured under well-defined and controlled conditions. Consequently,

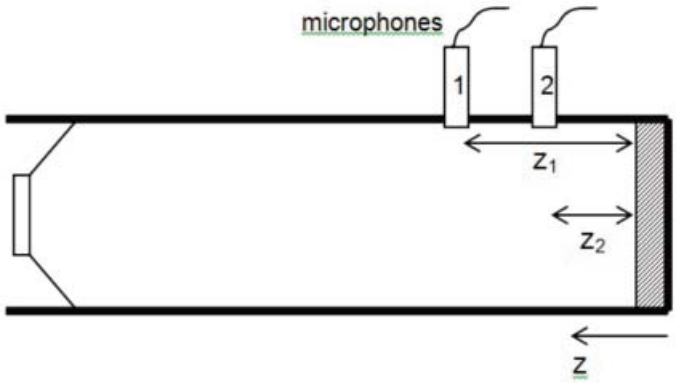

Figure 3.2.2 Two microphone impedance tube setup

it is frequently used in validating prediction models for porous materials. This method has the advantage of only needing small samples; this makes it ideal for developers of materials, as the alternative is to construct large samples for reverberation chamber tests, which is more difficult and expensive.

Figure 3.2.2 shows a typical set-up, and the concept is as follows. A loudspeaker generates plane wave propagation in the impedance tube, the plane wave propagates down the tube before reflecting from the sample. A standing wave is set up within the tube. The impedance of the sample alters how sound is reflected, and by measuring the resulting standing wave, it is possible to calculate the normal incidence absorption coefficient and surface impedance of the sample. This is such a common technique in acoustics, that it has been enshrined in international standards.

The highest frequency, fu, that can be measured in a tube is then determined by:

$$f_u = \frac{c}{2d}$$

where d is the tube diameter or maximum width and c the speed of sound. This is a statement that there should not be any cross modes in the tube; the first mode appears when half a wavelength fits across the tube. This high frequency limitation means that to cover a wide frequency range, several different impedance tubes of different diameter or width are required. However, it is possible to measure at higher frequencies if multiple microphones are used across the width of the tube. This technique is exploited in CARI's 160 mm impedance tube. The sound field within the tube can be considered to be a sum of the plane wave and higher modes, in a similar way to how a room sound field is decomposed into its modes.

For the square 160 mm tube, four microphones can be placed as shown in Figure 3.2.3, and the measured signals summed . In this case the first three cross-modes in the tube in each direction cancel or are not measured, leaving the fourth order mode to dominate. This quadruples the

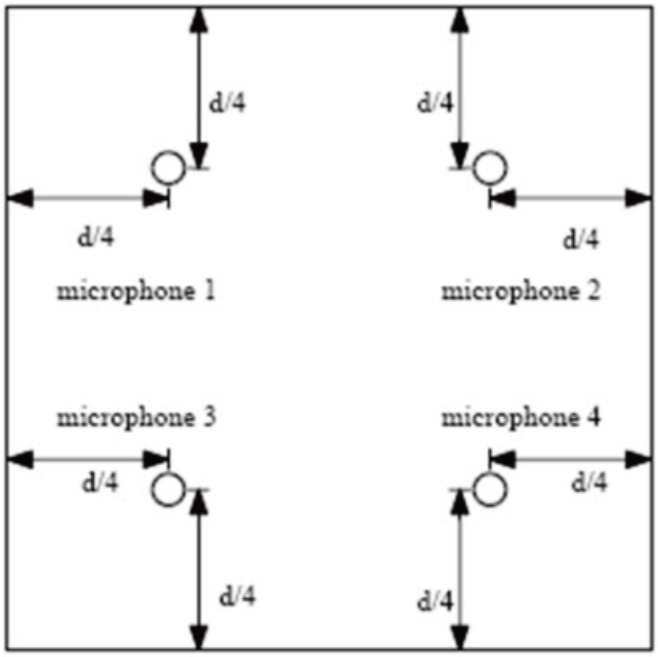

Figure 3.2.3.3 Multi-mic setup to quadruple upper frequency limit used in 160 mm impedance tube. This results in a useful range of 63-4000 Hz.

high frequency limit. Thus the 160 mm tube can measure up to 4,000 Hz third octave band.

If plane waves are assumed to propagate in the tube, then the steady state pressure in the tube is given by:

$$p = A\left(e^{jkz} + \mathrm{Re}^{-jkz}\right)$$

where R is the reflection coefficient; k is the wavenumber; the sample is assumed to be at z = 0, and A is a complex constant. The first term represents the incident wave, and the second the reflected wave.

The steady state pressure equation has two unknowns, the magnitude and phase of the reflection coefficient. By measuring the pressure at two points in the tube, it is possible to set up and solve simultaneous equations for the reflection coefficient and from there get the impedance and absorption coefficient. This is the principle of the transfer function, often called the two-microphone, method. (Although, as this is often used with one microphone which is moved, calling this a two-microphone method is nowadays rather misleading!)

The primary advantage of using this approach is that it obtains the absorption coefficient and impedance of the surface for all frequencies (within limits) with only a couple of quick measurements. The transfer function between two microphone positions in the tube is measured as shown in Figure 4.2. Remembering that the transfer function is simply the ratio of pressures, H12 = $p(z_2)/p(z_1)$, and applying the steady state pressure equation, the transfer function between microphone positions 1 and 2 is given by:

$$H_{12} = \frac{e^{jkz_2} + \mathrm{Re}^{-jkz_2}}{e^{jkz_1} + \mathrm{Re}^{-jkz_1}}$$

where z_1 and z_2 are the positions of the microphones shown in Figure 4.2. Rearrangement then directly leads to the complex pressure reflection coefficient:

$$R = \frac{H_{12}e^{jkz_1} - e^{jkz_2}}{e^{-jkz_2} - H_{12}e^{-jkz_1}}$$

The need for continuity of particle velocity normal to the surface enables the derivation of an expression for the specific acoustic impedance of the surface. The relationships between pressure reflection coefficient and impedance for normal incidence is given by:

$$\frac{z_1}{\rho c} = \frac{1+R}{1-R}$$

The absorption coefficient, α, is a ratio of the absorbed and incident energy enables the following expression to be derived:

$$\alpha = 1 - |R|^2$$

where |R| is the magnitude of the pressure reflection coefficient.

The 160 mm impedance tube provides absorption over the frequency range 63 - 4000 Hz as is seen in the measured absorption coefficient and impedance of a 2” fiberglass panel covered with a standard Guilford FR701 panel fabric in Figure 3.2.4.

The 610 mm square tube uses a single micro-

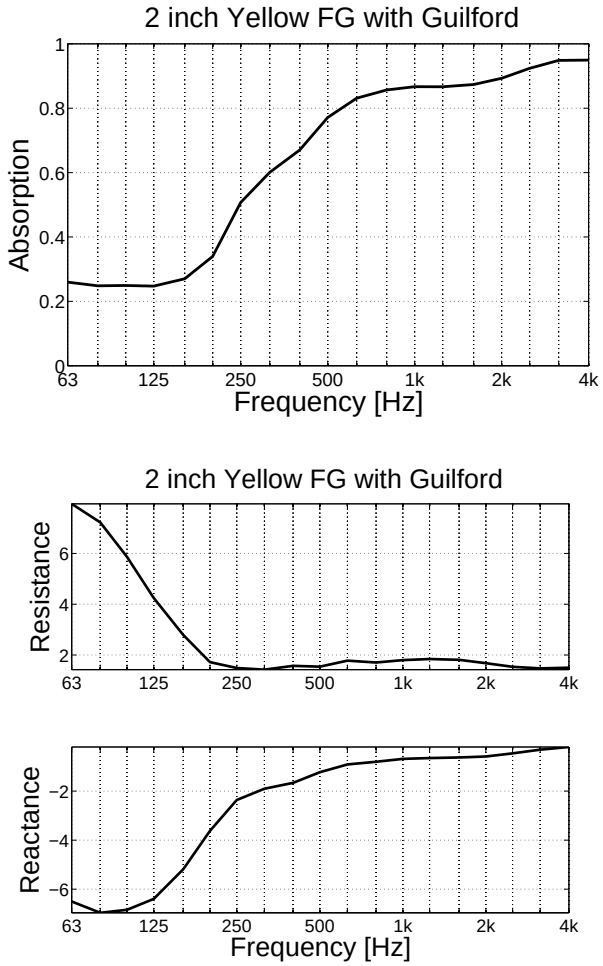

Figure 3.2.4. Absorption coefficient and impedance of a 2" fiberglass panel covered with a standard Guilford FR701 panel fabric measured in the 160 mm impedance tube.

phone, which is moved to three measurement positions. At each position the impulse response is measured to provide three overlapping transfer functions, from which the absorption coefficient is determined in the frequency range 20 Hz to 200 Hz. An example of a measurement of a resonant system in the 610 mm tube is shown if Figure 3.2.5.

A study of the low frequency behavior of Topperfo 16/16/8 was carried out in the 160 mm tube. The 17 mm panel contains 8 mm holes spaced 16 mm in orthogonal directions. The Topperfo sample was first mounted in a sealed box with a 4" air cavity. A 1" 6 pcf fiberglass panel was mounted directly to the rear surface of the Topperfo panel. The graph (Topperfo 4" Cavity A) shows a gradually rising absorption starting at roughly 50 Hz. The panel with the attached rear

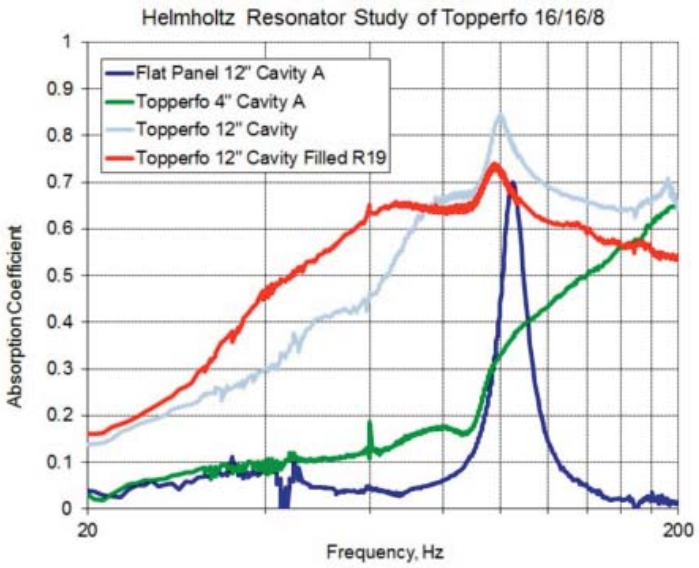

Figure 3.2.5. Helmholtz resonator study of a perforated panel.

1" fiberglass panel was then mounted in a sealed box with a 12" air cavity (Topperfo 12" Cavity). The light blue line shows significantly higher low frequency absorption with a value of roughly 0.65 from 250 Hz to 75 Hz followed by a rapid decrease. Also apparent was a resonance peak at 100 Hz. The air cavity of the box was then filled with R19 low density insulation and the measurement repeated (Topperfo 12" Cavity Filled R19). The absorption between 100 Hz and 250 Hz dropped as seen in the red curve, but the low frequency absorption below 75 Hz increased. The resonance at 100 Hz was still visible. To understand the nature of the resonance a flat non-perforated panel of similar thickness and density was measured in the 12" sealed box without R19 insulation (Flat Panel 12" Cavity A). This demonstrated clearly that the 100 Hz resonance was due to diaphragmatic panel resonance. The experiments indicate that significant low frequency absorption can be obtained using Topperfo, if a 12" or larger air cavity is employed, demonstrating the utility of the 160 mm impedance tube.

4 SCATTERING COEFFICIENT MEASUREMENT PROCEDURES

4.1 ISO 17497-1: Random Incidence scattering coefficient

The principle of a scattering coefficient is to separate the reflected sound into specular and scattered components. The specular component is the proportion of energy which is reflected in the same way as would happen for a large plane surface. The scattered components give the energy reflected in a non-specular manner. This is illustrated in Figure 4.1. The coefficient has a clear physical meaning, and the definition is very useful for geometric room acoustic models because these tend to have separate algorithms dealing with specular and scattered components, and so

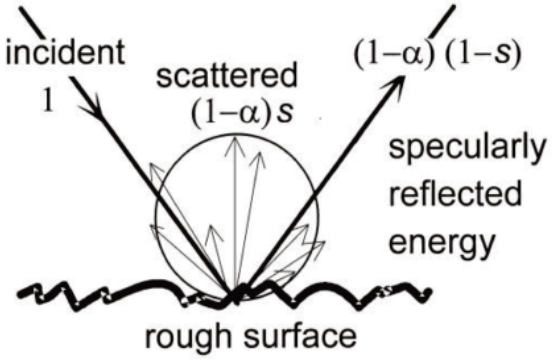

Figure 4.1. Graphic showing how incident sound, normalized to 1, can be specularly reflected and scattered. The scattering coefficient, s, determined the distribution.

the separation of terms mimics the modeling methods. With this definition it is then possible to define a scattering coefficient, s, as the proportion of energy not reflected in a specular manner.

This definition takes no account of how the scattered energy is distributed, but assumes that in most room acoustic applications there is a large amount of mixing of different reflections, and so any inaccuracies that arise from this simplification will average out. This is probably a reasonable assumption for the reverberant field, where there are many reflections, but could well be troublesome for the early sound field, where the impulse response is dominated by a few isolated reflections, and the correct modeling of these is essential to gaining accurate predictions. The scattering coefficient, like the diffusion coefficient, generally depends on frequency and angle of sound incidence. Similar to the random incidence absorption coefficient obtained in reverberation rooms, an angular average of the scattering coefficient - the random incidence scattering coefficient - can be defined. As a general assumption, the surface under test is assumed to be large and not too rough. The method will not work for isolated items and deep surfaces as it is trying to measure the scattering from the surface roughness and not the edges. It also has problems when the surface absorption is high, as the coefficient estimation becomes inaccurate.

With this definition it is then possible to define a scattering coefficients, s, as the proportion of energy not reflected in a specular manner.

The derivation of the scattering coefficient is given in Figure 4.2. While ISO 17497-1 calls for the use of the Sabine equation, we also calculate the absorption coefficients using Eyring, as described in 3.1. The four reverberation

$$a_s = 55.3\frac{V}{S}\left(\frac{1}{c_2 T_2} - \frac{1}{c_1 T_1}\right) - \frac{4V}{S}(m_2 - m_1)$$

$$a_{spec} = 55.3\frac{V}{S}\left(\frac{1}{c_4 T_4} - \frac{1}{c_3 T_3}\right) - \frac{4V}{S}(m_4 - m_3)$$

$$s = \frac{a_{spec} - a_s}{1 - a_s} = 1 - \frac{E_{\text{spec}}}{E_{\text{total}}}$$

Figure 4.2. Derivation of the scattering coefficient s.

	Stationary	Rotating
Table only	T_1	T_3
Table and sample	T_2	T_4

Table 4.1 The measurement conditions for the four different reverberation times.

times that must be measured are shown in Table 4.1. It is important to point out that in the determination of as and aspec, the absorption of the stationary and rotating table without sample is used as a reflective reference to adjust for table absorption. This will be referred to when we suggested using a reflective reference to determine the absorption coefficient according to ISO 354. The specular absorption coefficient is easiest to explain in the free field, although it is in the diffuse field measurement where this method is useful and powerful. The specular absorption coefficient is found by rotating the test sample while phase lock averaging the reflected pulses. Figure 4.3 shows filtered impulse responses at 100 Hz, 500 Hz and 2 kHz at two different positions of the rotating table in a reverberation chamber for a 1:1.5 scale Skyline 2-dimensional diffusor, shown in Figure 4.4 The curves on the left show the first 20 ms of the impulse responses, where the scattering is in phase. The initial parts of the reflections are highly correlated; these are the specular components of the reflection, and remain unaltered as the sample is rotated. In contrast, the later parts of the three reflected pulses, shown on the right between 200 and 210 ms, are not in phase and depend strongly on the specific orientation; this is the scattered component. By averaging the reflected impulse pres-

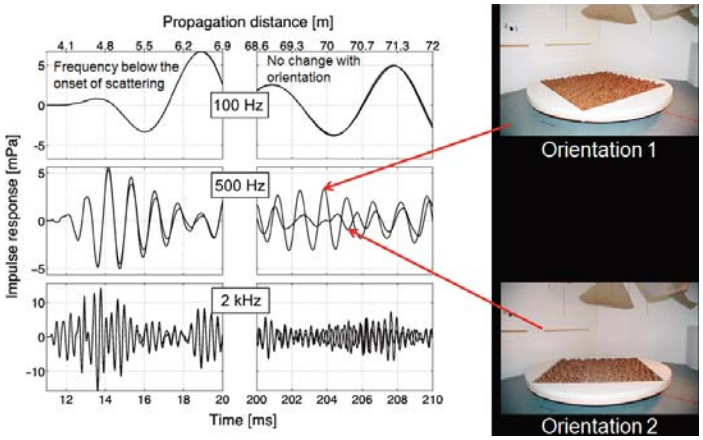

Figure 4.3. The impulse response is shown at two different rotating table positions at 100 Hz, 500 Hz and 2 kHz for a 1:1.5 scale Skyline. Left: First 20 ms; Right: 200-210 ms.

sure while rotating the sample, the scattered components are averaged to zero, and only the specular energy remains.

In the rev room a circular test sample, or a square sample surrounded by eyebrows, is placed on a turntable and rotated. While the turntable is rotated the room impulse response is repeatedly measured. The latter parts of the impulse response, which are due to the scattering from the

Figure 4.4. 1:1.5 Skyline on the rotating table in the rev room.

surface, will cancel out, and the averaged impulse response only contains the specular reflection component. This impulse response is then backward integrated to give the reverberation time due to the specular reflection component. The reverberation time with the sample stationary (not rotating) can also be obtained, and this decay is due to the total scattering - specular plus diffuse. By manipulating these reverberation times, it is possible to derive the specular and total reflected energy, and from the Equations in 4.2 the scattering coefficient.

To achieve adequate coherent averaging, it is recommended that 72 averages be made during a table rotation.

Therefore, if one uses a 3 s MLS stimulus, a table rotation will take 3.6 m, with a 0.3 rpm. We have installed a high quality rotating table, shown in Figure 4.4, with a metal frame to support the table to insure it is flat. This frame is then covered with a flat and lacquered base table on which samples are located.

To satisfy ISO 354 in determining reverberation times, we employ 6 distributed stationary mics and two loudspeakers in opposite trihedral corners. Each rotating table experiment requires the measurement of 12 impulse responses for each table revolution. 12 times 3.6 m is 43 m. Thus the rotating table measurements, T3 and T4, require 90 minutes. Measurement of T1 and T2, sample mounting and delays for opening and closing the chamber door will add additional time, so the entire measurement can be quite time consuming, while monitoring temperature and pressure. To greatly accelerate the measurement process, we energize both loudspeakers and simultaneously measure the 6 impulse responses using EASERA and a MOTU 8Pre. With this approach, each rotating table measurement is reduced from 43 m to 3.6 m, as shown in Figure 4.5.

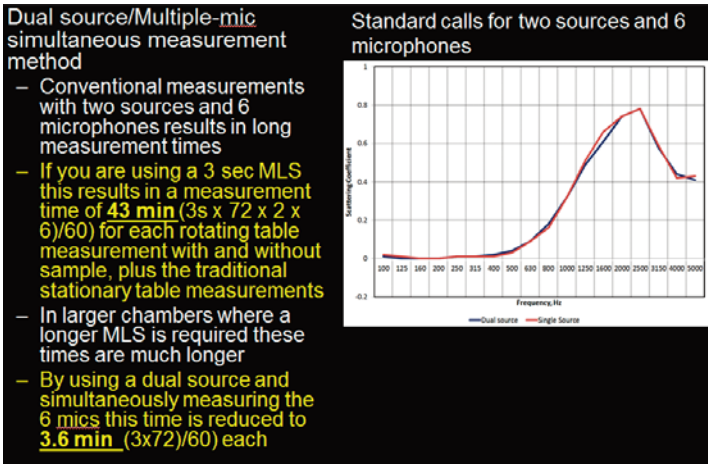

Figure 4.5. Comparison between single source and dual source/multiple-microphone measurement of the scattering coefficient. The agreement is excellent and the time reduction is quite dramatic.

To verify the accuracy of our measurements, we have measured samples studied in other laboratories in a round robin at various scales. A simple round robin sample is a set of periodic battens, shown on the base table.

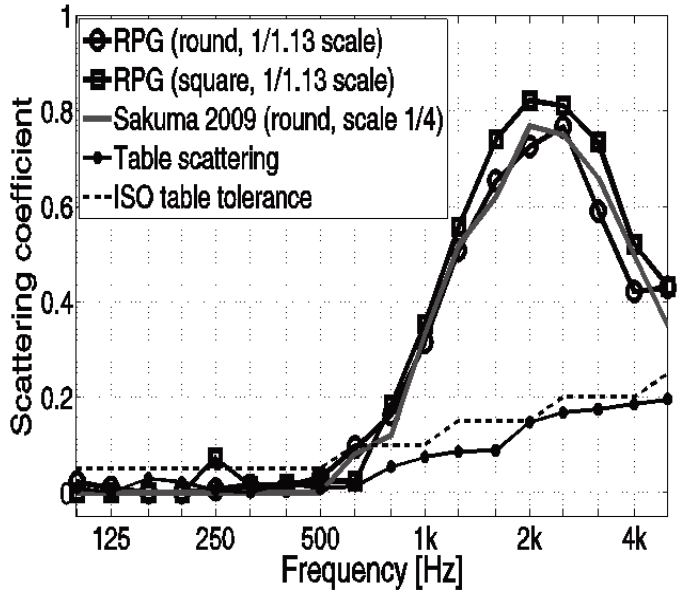

Table 4.6. Left Top: Rotating table frame; Middle: Metal frame covered with sealed table top; Bottom: Table top covered with a circular array rectangular battens; Right Top: Table top with eyebrows to support a rectangular array of battens; Middle: Battens in the square sample area; Bottom: Scattering coefficient comparison with another laboratory at various scales, showing excellent agreement. The dotted line indicates the upper limit for the rotating table scattering.

In Figure 4.6 we show the setup and measured scattering coefficients for two mounting conditions and comparison with other laboratories that have measured the rectangular battens. The sample can either cover the entire circular table or mount in a square sample area created by "eyebrows" the cover the rest of the table. This setup is very convenient for commercial samples that are square. On the left side we see the table metal frame (top) to provide stability for the sealed table top supporting the sample (middle) and the batten samples filling the entire circular

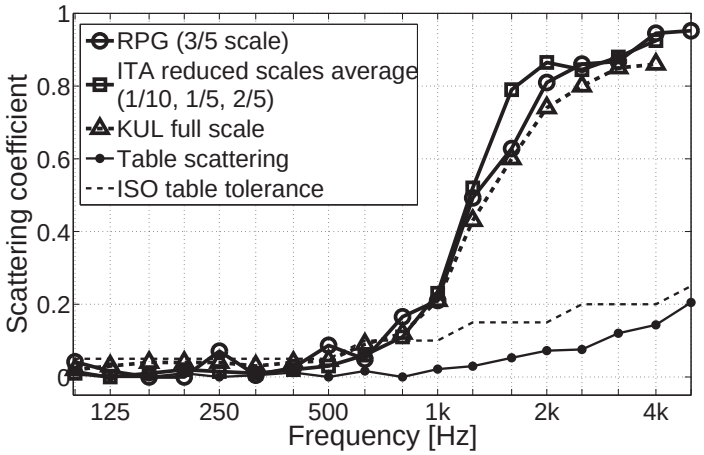

Table 4.7. Top: Empty table; Middle: Sinusoidal sample on table; Bottom: measurement results, comparison with other laboratories and table scattering.

table (bottom). On the right side, we see the table top with "eyebrows" (top), the square sample array of batten (middle) and the scattering coefficient results compared with other laboratories. We show the RPG (round 1:1.13 scale), RPG (square 1:1.13 scale) compared to the results obtained by Sakuma (University of Tokyo) in 2009 for the round mounting at 1:4 scale. The agreement is excellent. In Figure 4.4 we also show the ISO table tolerance limit for the table scattering indicated by the dashed line. It can be seen that the measured table scattering is below this limit.

In Figure 4.7, we show the setup and results obtained for another round robin sample, a sinusoidal surface. At the top we show a somewhat smaller empty table, the sinusoidal sample in the middle and the results and comparison at the bottom. The RPG sample is in 3/5 scale, while the ITA (Institute of Technical Acoustics, Aachen, Germany) sample is an average of 1/10, 1/5 and 2/5 scale and the KUL (University of Lueven, Belgium) sample is measured full scale. We also verify that the table scattering is well below the ISO table tolerance.

An additional measurement can be seen in Figure 4.8, for a 1:1.5 Skyline two-dimensional diffusor. The empty table is shown at the top with the square sample mounting. The square array of Skylines is shown in the middle filling the square sample area. The results indicate no significant difference for a periodic and aperiodic mounting of the Skylines. Table scattering is below the ISO table tolerance.

In Figure 4.9, we illustrate how a sample can have a good scattering coefficient, meaning significant energy is scat-

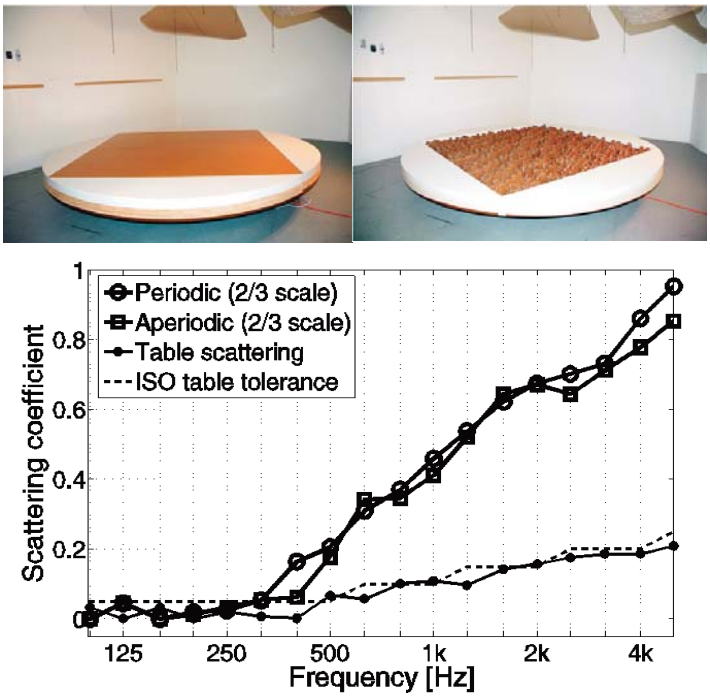

Figure 4.8. Top: Empty table; Middle: 1:1.5 scale Skylines in square sample mount; Bottom: scattering coefficients for periodic and aperiodic mounting.

tered away from the specular zone, while having a poor diffusion coefficient, meaning the scattered energy is not uniformly distributed. In the figure we show the batten sample with a period or structural wavelength of 177 mm in the upper left, the polar responses for the batten (red) and a flat reference reflector (blue) for an angle of incidence of 300 at 2000 Hz. The specular zone is also shown. In addition the scattering coefficients, s, determined according to ISO, Correlation and Energetics and the normalized diffusion coefficient, dn, are also shown. The three scattering coefficients all peak at roughly 0.8 at the frequency of the

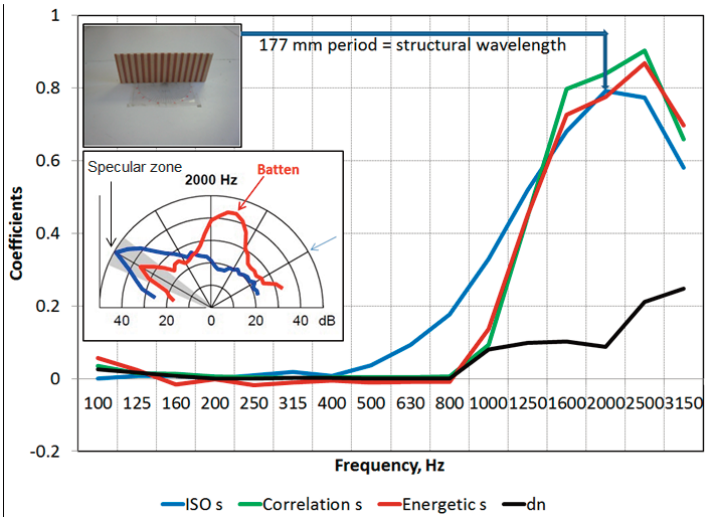

Figure 4.9 The batten polar response at the structural wavelength frequency of 2000 Hz illustrates why the scattering coefficient is high in that energy is scattered away from the specular zone. It also shows why the diffusion coefficient is poor and non-uniform.

structural wavelength, 2000 Hz. However, the diffusion coefficient is much lower. The explanation lies in the polar responses. The batten scatters incident sound away from the specular zone, giving rise to a good scattering coefficient, but the batten polar response is quite non-uniform, leading to a poor diffusion coefficient. The moral is to use each coefficient for what it was intended, i.e. use the scattering coefficient in computer room modeling programs and the diffusion coefficient to evaluate the uniformity of diffusion for diffusor design or to compare potential diffusing surfaces. Often scattering coefficients are used in specifications to compare diffusors, which is an improper use.

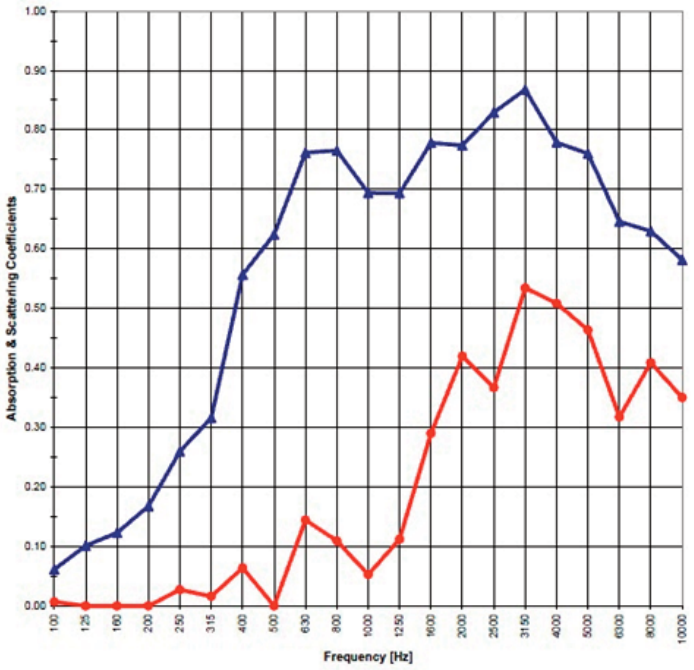

Figure 4.10 This is an example of absorption (blue) and scattering (red) data presented in a specification and represents a misuse ISO 17497-1, because the standard specifically states that the test is invalid for samples having an absorption coefficient greater than 0.5.

Another misuse of the scattering coefficient is to measure it for surfaces which have absorption in excess of 50%. In Figure 4.10, we show results presented in a project specification for a product billed as an absorber and diffusor, based on the scattering coefficient data. This is incorrect on two accounts. The measurement of the scattering coefficient is invalid, due to excess absorption, and the data are misinterpreted to indicate the product is a diffusor, based on the scattering coefficient rather than the diffusion coefficient, which is not presented.

At 3150 Hz, the absorption coefficient is 0.87, which means there is 13% of the incident energy left to be scattered. The scattering coefficient, which is incorrect according to ISO 17497-1 because absorption is greater than 0.5, is 0.53. Ignoring the fact that it is incorrect for the moment, this means that 6.9% of the scattered energy is directed in non-specular directions. While the product is a good absorber, it is certainly not a good diffusor.

4.2 Correlation Scattering Coefficient From Polar Responses

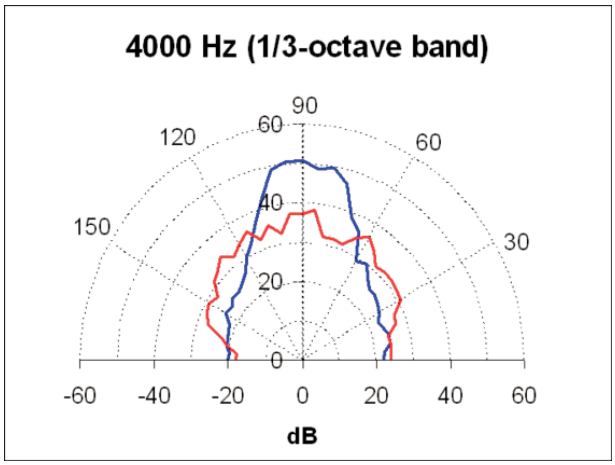

Figure 4.11. Comparison between the polar response of a flat reflector (blue) and the sample (red) at 4 kHz third octave band.

Because the ISO method uses a rotation of the sample to cancel out the non-specular components, it cannot distinguish between scattering surfaces that contain depth variation in one direction (1D diffusors) and those with depth variation in two directions (2D diffusors). Two methods have been developed to obtain the scattering coefficient from measured or calculated polar responses, which do differentiate between 1D and 2D surfaces.

Mommertz presented a method for evaluating a scattering coefficient from polar responses, Figure 4.11. This correlates the scattered pressure polar responses from the test surface and a reference flat surface to give a scattering coefficient. This will be called the correlation scattering coefficient sc. The coefficient is given by:

$$s_c = 1 - \frac{\left|\sum_{i=1}^{n} p_1(\theta_i)\, p_0^*(\theta_i)\right|^2}{\sum_{i=1}^{n} |p_1(\theta_i)|^2 \sum_{i=1}^{n} |p_0(\theta_i)|^2}$$

where p1 is the pressure scattered from the test surface; p0 is the pressure scattered from the flat surface; * denotes complex conjugate; qi the receiver angle of the ith measurement position, and n is the number of measurements in the polar response. This is not the same as the ISO coefficient or the free field scattering coefficient. The difference arises because the coefficient definition is different. The free field Mommertz and Vorländer method measures the amount of energy moved from the specular direction when the surface is moved, the correlation scattering coefficient measures the dissimilarity between the test and flat surface scattering over a polar response. In the case of randomly rough surfaces, the two coefficients probably are similar, but for diffusers with distinct polar responses, this is not the case. The random incidence correlation scattering coefficient is approximated by averaging over the angles of incidence to determine an average incidence coefficient.

4.3 Specular Zone or Energetic Scattering Coefficient from Polar Responses

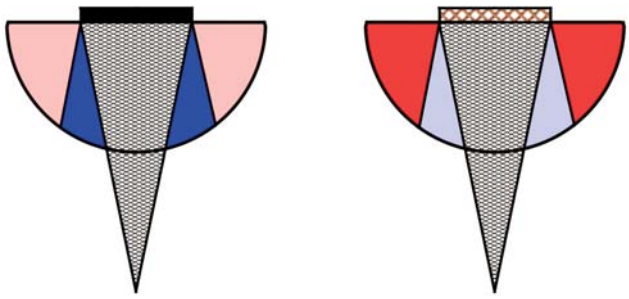

Figure 4.12. (left) Specular zone for a reflector in dark blue and the diffuse zone in light red; (right) Specular zone for a diffusor is shown in light blue and the diffuse zone in dark red, indicating energy is scattered out of the specular zone into the diffuse zone.

A second method has been developed to distinguish scattering coefficients between 1D and 2D surfaces, utilizing the specular zone. Paralleling the definition of the ISO scattering coefficient, one can calculate the specular energy, Espec, by measuring the energy in the specular zone of a polar response. The total energy, Etotal, can also be determined from the total energy under the polar response. The specular zone is shown in Figure 4.12 on the left in dark blue for a reflector. The diffuse zone is shown in light red. If the scattering sample is a diffusor, some of the specular energy is scattered out of the specular zone, light blue, into the diffuse zone, dark red, increasing the specular zone scattering coefficient, ssz, defined below. This specular zone measurement, ssz, will consider edge diffraction and surface roughness as diffusion. To eliminate the edge diffraction, one can subtract the specular zone scattering coefficient of a reflector panel of similar size, ssz(r), from the specular zone scattering coefficient of a diffusing surface, ssz(d), and normalize by [1-ssz(r)], to provide a normalized specular zone scattering coefficient, sn,sz. Data from various angles of incidence can be averaged to obtain an average incidence specular zone scattering coefficient.

$$s_{sz} = 1 - \frac{E_{specular\ zone}}{E_{total}}$$

$$s_{n,sz} = \frac{s_{sz}(d) - s_{sz}(r)}{\left[1 - s_{sz}(r)\right]}$$

5 DIFFUSION COEFFICIENT

RPG has played a leading role in the establishment of two proof of performance metrics, which evaluate the performance of sound diffusing surfaces. The Scattering Coefficient, s, is a quantity metric, and is the ratio of sound energy scattered in a non-specular manner to the total reflected sound energy. It is described in ISO 17497-1. The Diffusion Coefficient, d, is a quality metric, and is a measure of the uniformity of the reflected sound. It is described in AES-4id-2001, soon to be incorporated as ISO 17497-2. The Scattering coefficient is used in modeling programs along with the random incidence absorption coefficient. The Diffusion Coefficient is used by manufacturers to design diffusing surfaces and by specifiers to evaluate potential diffusing surfaces .

5.1 Measurement and data reduction

In 2001, the AES Standards Working Group SC-04-02 published an information document, based on peer review of a committed of international acousticians, which described a method to measure and characterize how uniformly a surface scatters sound. The measurements are carried out with a boundary layer goniometer, shown in Figure 5.1, in which 37 sequential impulse response measurements were made, using 37 fixed pressure zone microphones and an MLS excitation signal under computer control. Figure 8 illustrates the sequence of events in determining the scattered impulse response at a particular observation angle, for a given angle of incidence. To obtain the impulse response of a sample under test, it is necessary to de-convolve the loudspeaker-microphone response at each scattering angle, h3(t). It is also necessary to minimize any room interference and reflections from microphone supports and wires within the time window of interest. To obtain the "Loudspeaker/Microphone Response" (top panel in Fig. 5.2) at each scattering angle, the loudspeaker is placed at the sample position and rotated so its on-axis response is coincident with the on-axis response of each microphone for each angle.

The loudspeaker is then placed in its normal source position, without any sample present, and the "Background Response Without Sample", h2(t), at each angle is

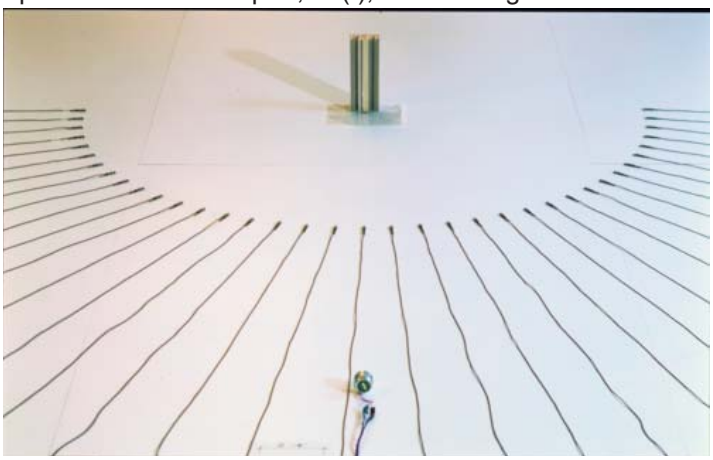

Figure 5.1. 2D diffusion goniometer showing loudspeaker, microphone array and sample.

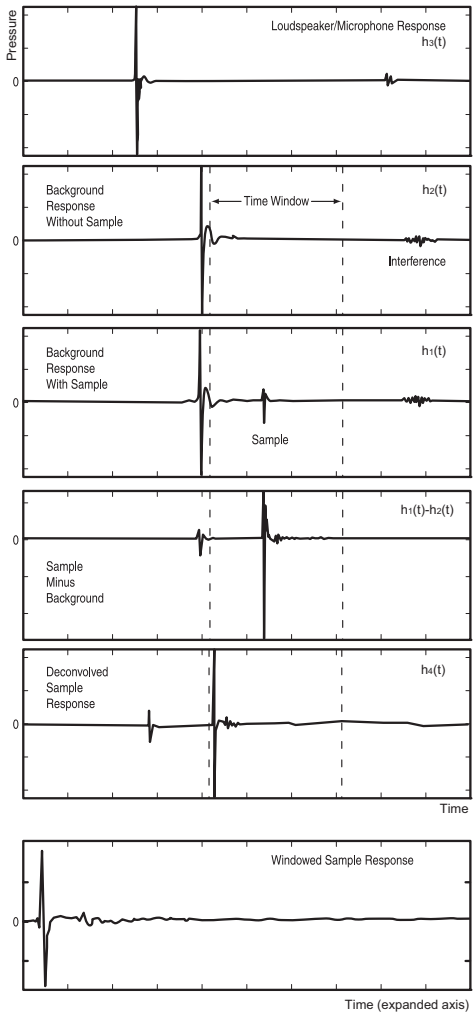

Figure 5.2. Data reduction process to extract the scattered impulse response from a test sample at a given observation angle.

automatically measured via computer control by emitting 37 impulses and sequentially switching each microphone on. A vertical dotted line representing the "Time Window" of 10 ms, used to isolate the reflections, is also shown. The sample under test is then placed in position and the scattered sound is measured, obtaining the "Background Response With Sample", h1(t), in Figure 5.2.

Data are collected at 50 intervals. Higher resolution, for example 2.50, is possible by combining another data set with the sample rotated by 2.50. In the sequential approach, the measurement system selects a microphone, emits a selected maximum length sequence stimulus, records the data, selects the next microphone position, etc. Since the microphones are stationary and the measurement process is rapid, the respective background response can be subtracted from each microphone position, prior to de-convolution. This is illustrated as "Sample Minus Background" in Figure 5.2. The direct sound is significantly decreased and is not providing interference in the time window with the scattered sound.

The room interference is also decreased. The speaker/microphone response can now be de-convolved as illustrated in "De-convolved Sample Response", h4(t), where h4(t) is calculated using:

$$h_4(t) = IFT \left[\frac{FT\ [h_1(t) - h_2(t)]}{FT\ [h_3(t)]} \right] \qquad (1)$$

where FT and IFT are the forward and inverse Fourier transforms. The data within the Time Window is gated to isolate the "Windowed Sample Response".

The data are further post processed to provide frequency responses, polar responses and finally diffusion coefficients, as shown in Figure 5.3, with a reference reflector on the left and a diffusor on the right. The 2D boundary measurement geometry with the loudspeaker at -600, with respect to the normal is shown in Figure 5.3A at the top of the figure. Also shown are the 37 receiving microphones and a scattering sample at the origin of the mic and speaker semicircles. Below that, Figure 5.3B, the impulse response at 600 is shown, with the scattered data outlined in a box, corresponding to the time window in Figure 5.2. The scattered data are windowed for all of the angles of observation, of which five are highlighted at -60, -30, 0, 30 and 600 and concatenated in Figure 5.3C in the form of a temporal angular impulse response. A Fourier Transform is then applied to each part of the impulse response to get the frequency responses, Figure 5.3D. Five of the 37 frequency responses are only shown for clarity. The frequency response energy is summed over one third octave bands and

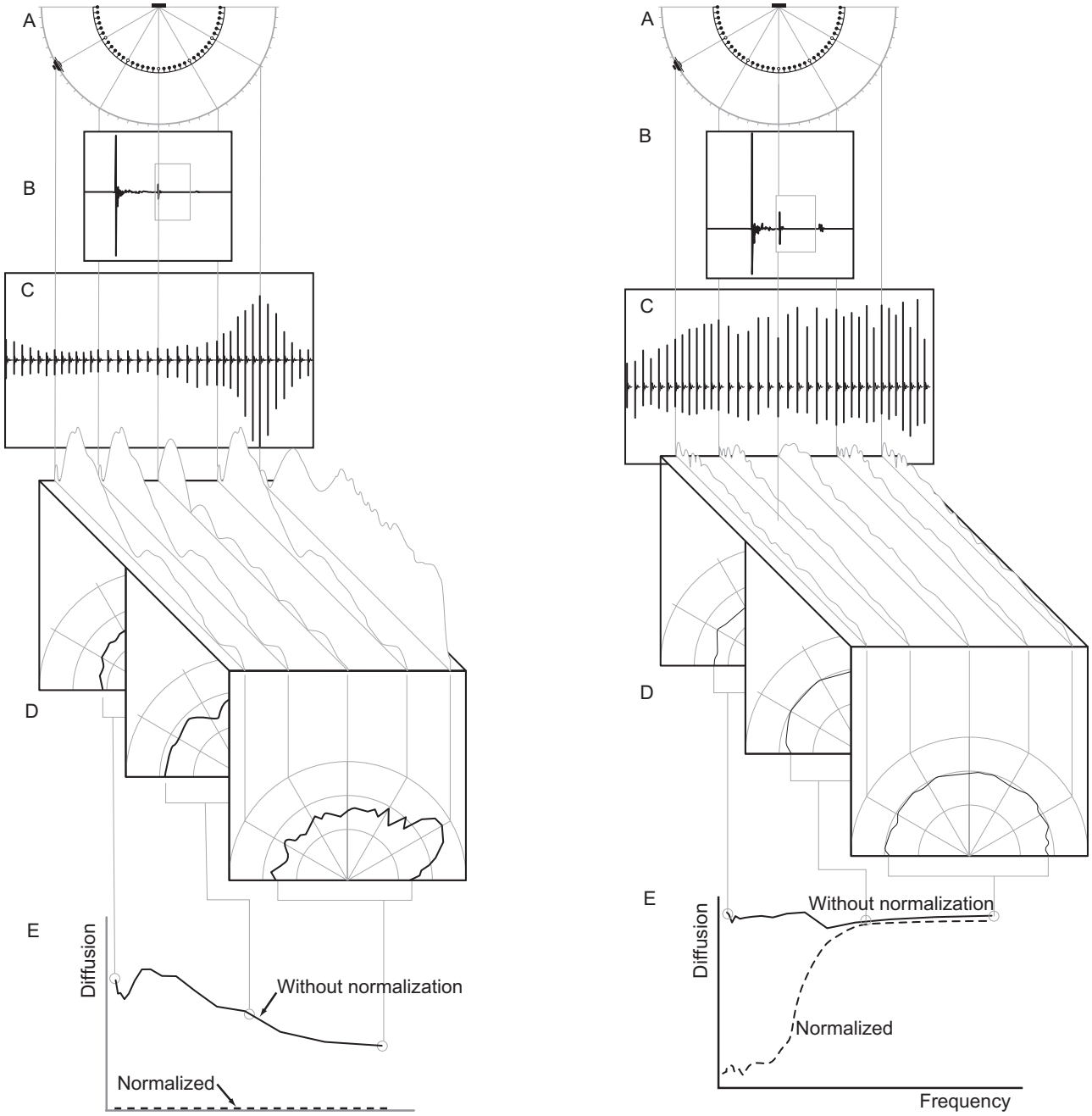

Figure 5.3. Left: Summary of data processing technique from a flat reflector at -60⁰ incidence. Right: Summary of data processing technique from a diffusor at -60⁰ incidence.

three of the polar responses are shown in Figure 5.3D. The visible polar response of the reflector, in the left panel, at high frequency is narrow and directed in the specular direction of +60, as would be expected, whereas the corresponding polar response for the diffusor is uniform. The polar responses can then be further processed to give a diffusion coefficient, which is plotted versus frequency to obtain the diffusion response, Figure 5.3E. As the frequency increases, one can see a drop in the diffusion coefficient of the reflector, as the width of the panel become increasingly large compared to the wavelength. The directional diffusion coefficient, dy, is determined from the autocorrelation of the third octave polar responses as described in Eq. (2): where

$$d_y = \frac{\left[\sum_{i=1}^{n} 10^{L_i/10}\right]^2 - \sum_{i=1}^{n} \left(10^{L_i/10}\right)^2}{(n-1)\sum_{i=1}^{n} \left(10^{L_i/10}\right)^2} \qquad (2)$$

Li are a set of sound pressure levels in decibels in a polar response, n is the number of microphones, y is the angle of incidence.

At low frequency, edge scattering causes the diffusion coefficient to increase with decreasing frequency, because the sample acts as a point source scattering onmidirectionally. While there is a clear physical explanation for this effect, it does lead to confusion, and so a normalized diffusion coefficient is introduced to remove this effect. The result of doing this is shown in Figure 5.4 for a few commercial products and a reference flat surface.. This gives the more intuitive response, with surfaces producing little diffusion at low frequency. It also more clearly illustrates the frequency where diffusion begins. The normalised diffusion coefficient, dy,n, is calculated using the following formulation:

$$d_{\psi,n} = \frac{d_\psi - d_{\psi,r}}{1 - d_{\psi,r}} \qquad (3)$$

where dy and dy,r are the diffusion coefficients calculated using Equation (2) for the test sample and a reference flat surface of the same overall size as the test sample. At low frequency, sometimes the normalized diffusion coefficient dips below zero, and in these cases, the negative values should be set to zero.

To accurately subtract the background impulse, h2(t), from the sample impulse, h1(t), we use the method developed by Philip Robinson (P. Robinson and N. Xiang, J. Acoust. Soc. Am. 127 (2010)), using oversampling. The two impulse responses are oversampled 100x and shifted until the residual is minimized. This is illustrated in Figure 5.5. In the top of Figure 5.5, we show the reference reflection (blue) and sample (red) minus the background response for a given observation angle, without oversampling, along with the polar responses. While the background subtraction from the sample is correct, the background subtraction from the reference reflector has left a significant residual, leading to spikes in the polar response (blue). In the lower part of

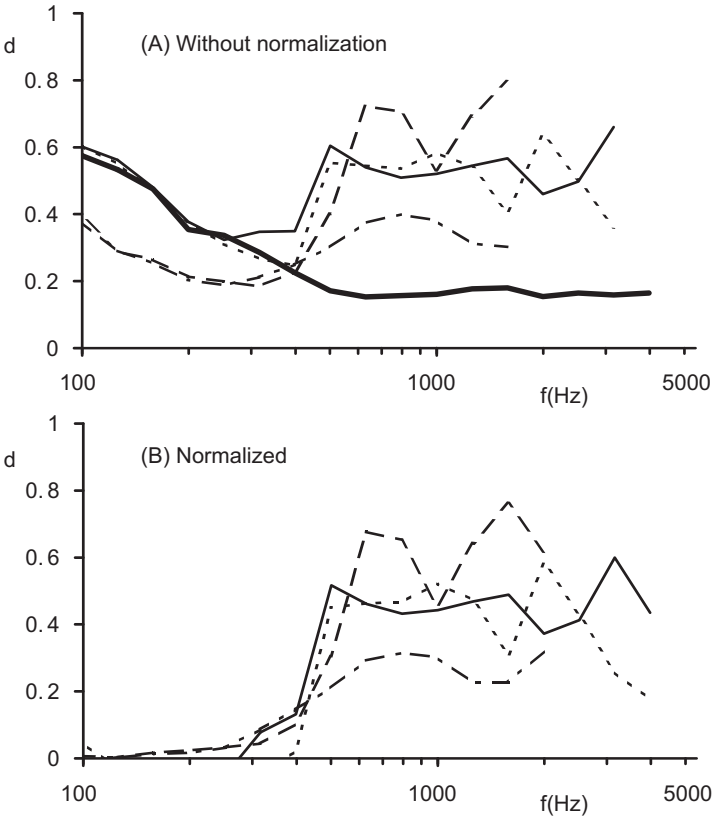

Figure 5.4 Diffusion coefficient for four commercial products. Top: not normalized; bottom: normalized. The thick line in the top picture is the diffusion coefficient for a flat reflector.

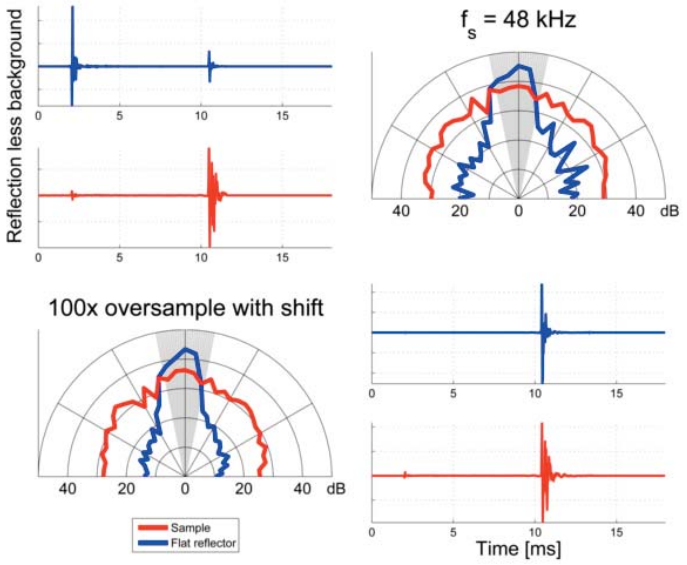

Figure 5.5. Top: Background subtraction without oversampling/shifting, shows residual direct sound in the reflection impulse response (blue) and resulting spikes in the reflector polar response . Bottom: Background subtraction with oversampling/shifting resulting in complete removal of the direct sound in the reflector and sample impulse responses, with accompanying smoothing of the reflector polar response.

Figure 5.5, we show how oversampling and optimal shifting completely removes the background scattering from the reference reflector, with resulting improvement in the polar response.

Recently several improvements have been made to the design of the measurement goniometer, the measurement hardware and software. These include:
- Software to optimize the microphone and speaker radii to allow for a 40% larger sample area while not increasing the specular zone
- Hardware and software to allow simultaneous measurement of 32 impulse responses to greatly accelerate measurement time
- New data reduction and analysis software

5.1.1 Goniometer Optimization

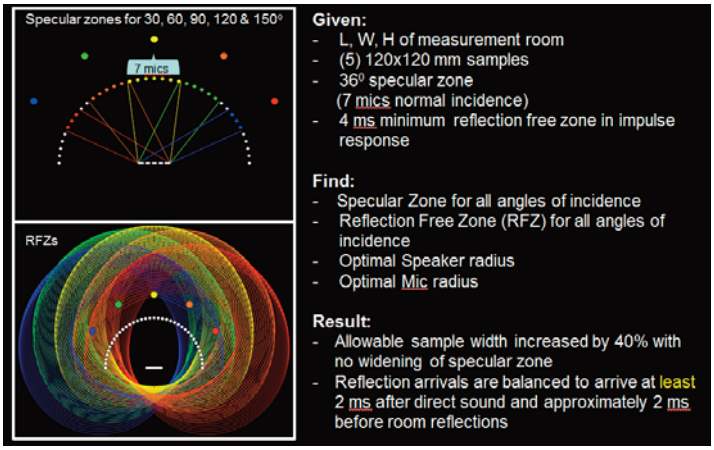

Figure 5.6 New goniometer dimensions optimized for given room size. Allowable sample width increased by 40% with no widening of the specular zone. Reflection arrivals are balanced to arrive at least 2 ms after direct sound and approximately 2 ms before room reflections.

The new goniometer optimization results are shown in Figure 5.6, in which we show the specular zones for 30, 60, 90, 120 and 150 degree incidence in the top of the figure and the reflection free zones (RFZs) in which there are no competing room reflections in the bottom of the figure. The main goal of the optimization is to determine the optimal mic and speaker radii to enable the measurement of (5) 1:5 scale samples (120 mm x 120 mm) maintaining a specular zone of 360 degrees (7 mics at 50 angular resolution) and a reflection free zone of 4 ms minimum in a room of a given length, width and height, for all angles of incidence.

5.1.2 Simultaneous Impulse Response Measurements

There have been continuing advances in data collection over the years. From 1983 to 1993, impulse response data were collected with a TEF analyzer using one microphone, which was manually repositioned with a 50 angular resolution after each impulse response measurement. Needless to say it was quite time consuming. This setup is shown in Figure 5.7 in a large sports arena. During this time measurements were made in full scale in arenas, gymnasiums and other large spaces in which we quickly wore out our welcome. In 1994, we decided to make measurements in scale and developed the first boundary plane goniometer utilizing 37 fixed mics every 50. In order to automatically sequence the microphones an Audio Precision mic switcher was used in conjunction with the TEF analyzer. Proprietary software automatically emitted 37 MLS stimuli and switched the microphones after an impulse response measurement. A photo of the goniometer, TEF and switcher can be seen in Figure 5.7 (right).

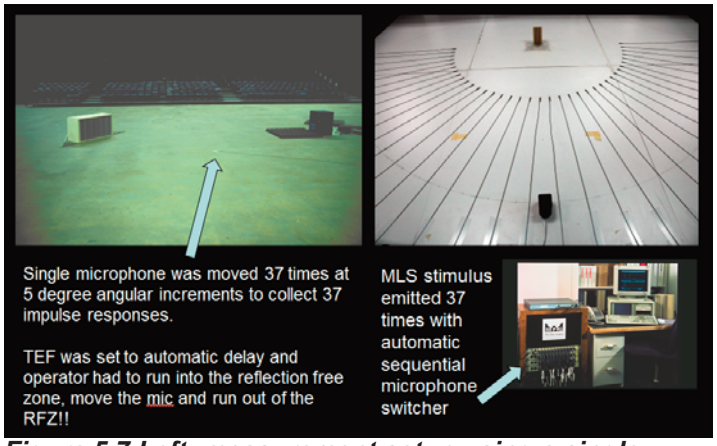

Figure 5.7 Left: measurement setup using a single, manually positioned microphone. Right: 1:5 scale boundary plane goniometer with 37 fixed microphones every 5⁰ with sample and loudspeaker. Mic radius was 1m and speaker radius was 2m. Under computer control we were able to sequentially collect 37 impulse responses.

In 2011, new hardware and software were added to collect 32 simultaneous impulse responses. This was accomplished using (4) MOTU 8Pre preamps and a hard disk

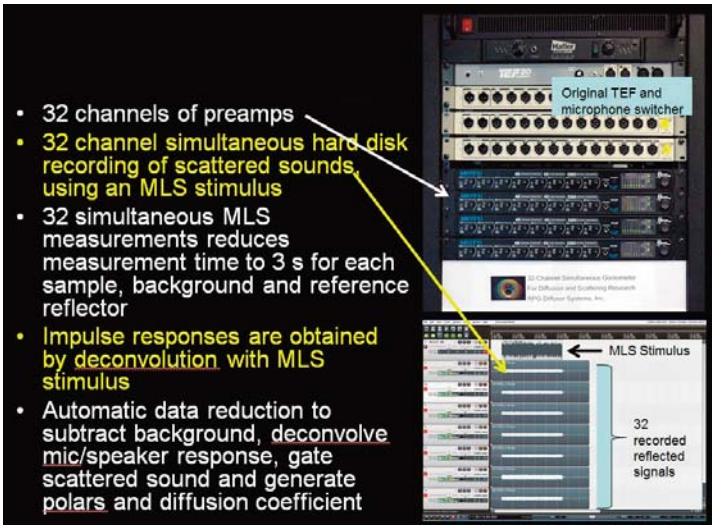

Figure 5.8The figure contains an equipment rack with, from top to bottom, the Hafler amplifier, the original TEF20 and microphone switchers used in previous measurements and the (4) MOTU 8Pres. Below that we show the hard disk GUI with MLS stimulus and some of the 32 recorded reflected signals, which were subsequently deconvolved to yield impulses.

recording program. An MLS signal was used as the stimulus and 32 channels of the scattered energy were recorded. This setup can be seen in Figure 5.8. From top to bottom, the rack contains a Hafler amplifier, a TEF20 and three 12 channel microphone switchers, previously used, and (4) MOTU 8Pre preamps. Below that we show the GUI of the hard disk recorder. At the top is the MLS stimulus followed by a few of the 32 recorded reflected signals. It was decided that rather than purchasing (5) 8Pres affording 40 preamps, we would settle for 32 channels and eliminate the extreme angular measurements, which did not yield significant information. To obtain the impulse responses, we deconvolved the recorded signals with the MLS stimulus. The impulse responses for all 32 channels are shown in Figure 5.9.

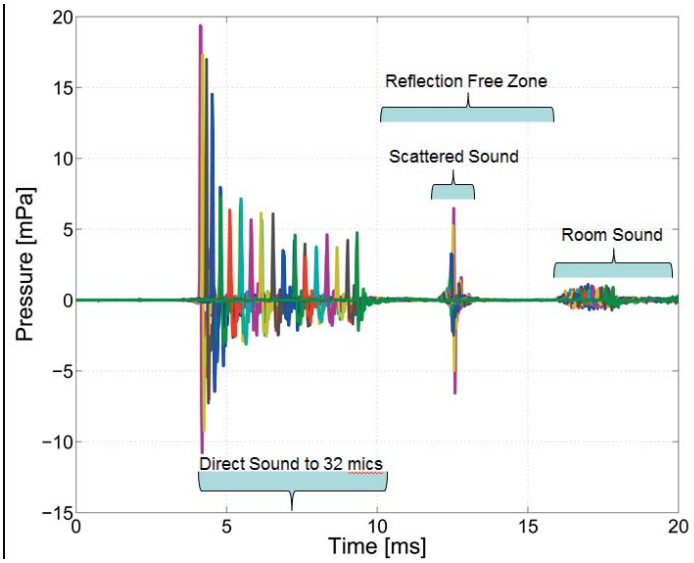

Figure 5.9 All 32 impulse responses are shown. The 32 direct sound impulses are shown as two overlapping sets of 16 signals, since the normal incidence setup is symmetrical. The 32 scattered impulse responses are nested in the center of the reflection free zone, followed by the interfering reflections from the room.

The simultaneously collected data were processed as described in section 5.1. Two continusous views of the narrow band polar data versus frequency are shown in Figure 5.10 for the reflector and sample. These data are subsequently filtered into third octave polars to determine the diffusion coefficient, as displayed in Figure 5.11, in which the photo of the round robin semicylinder array sample is shown upper left, the diffusion coefficients for the sample (red) is shown upper center and the normalized diffusion coefficient is shown upper right. 12 third octave polar responses are shown in the lower part of Figure 5.11, with red representing the sample and blue the reference reflector.

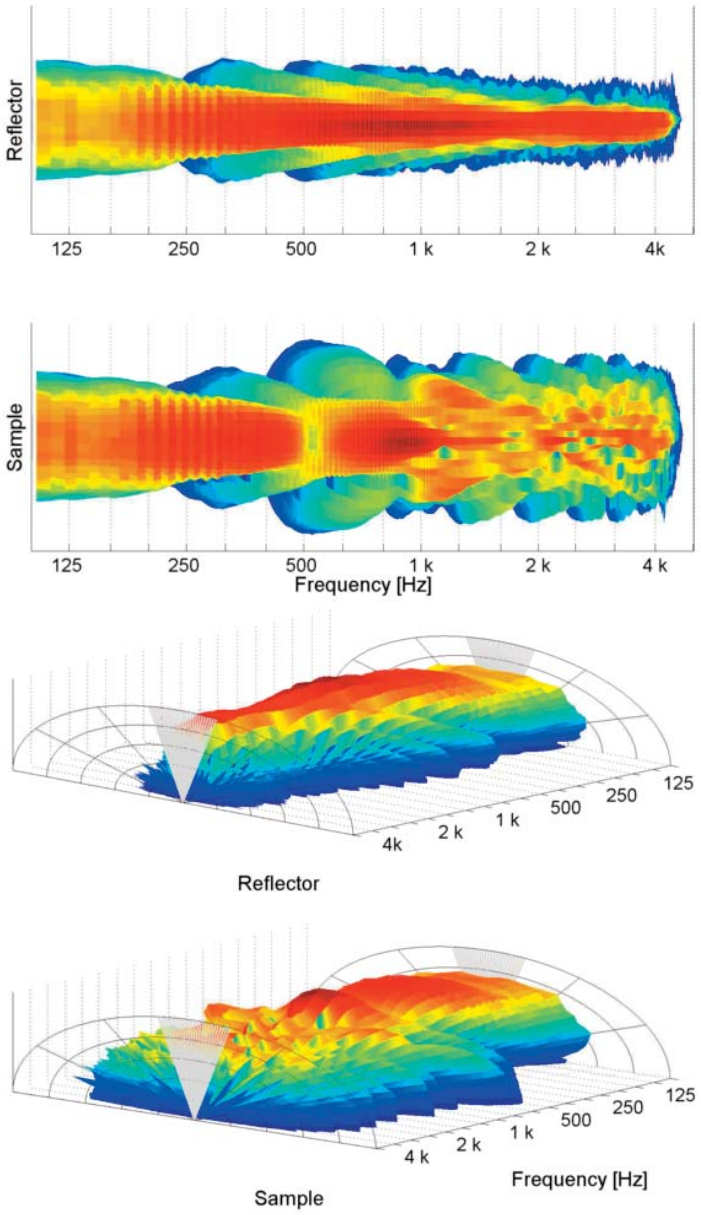

Figure 5.10 Narrow band polar displays, which are filtered into third octave bands to determine the diffusion coefficient and for efficient display specified in ISO 1749702, as illustrated in Figure 5.10.

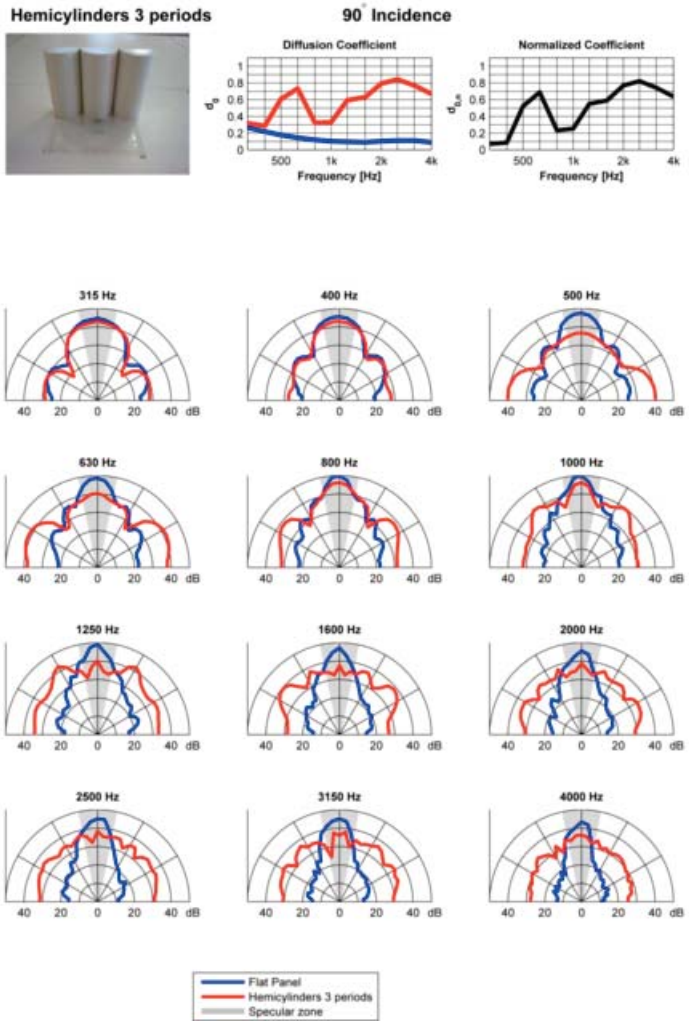

Figure 5.11 Presentation format as specified in ISO 17497-2. Upper left is a photo of the round robin hemi-cyinder array required for goniometer commissioning, upper middle is the diffusion coefficient of the sample array (red) and a reference reflector (blue). Below are 12 polar responses with sample in red and reflector in blue.

6 FABRIC TRANSPARENCY TESTING

Weaving is a textile craft in which two distinct sets of yarns or threads are interlaced to form a fabric or cloth. The threads which run lengthways are called the warp and the threads which run across from side to side are the weft or filling (Figure 6.1). Cloth is usually woven on a loom, a device that holds the warp threads in place while filling threads are woven through them.

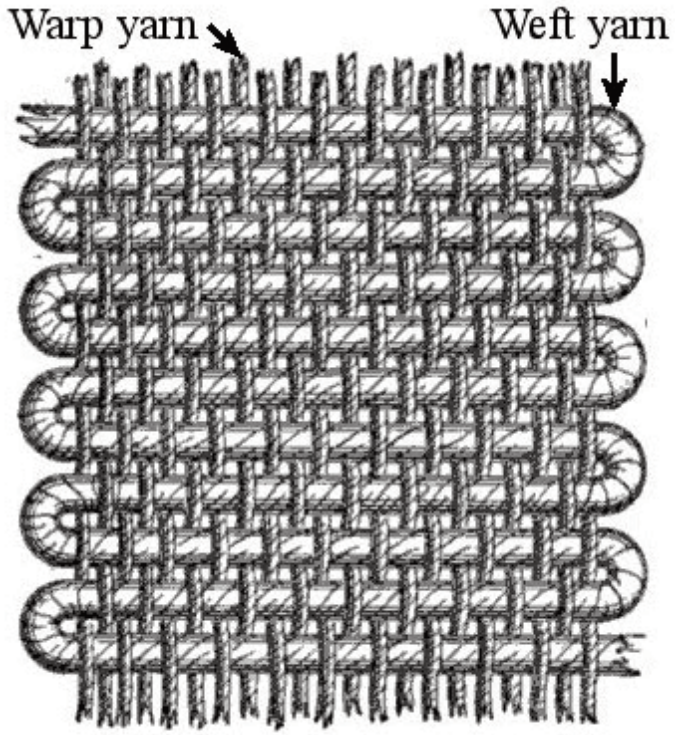

Figure 6.1. Illustration of the weaving pattern in a textile.

To visually investigate fabric weaving we can utilize a digital microscope with a magnification of 40X, Figure 6.2. The image from the microscope is captured on the laptop screen and distance measurements can also be made. The test fabric is placed on a light box to visualize spaces between the warf and the weft yarns. The fabric on the laptop screen is a standard panel fabric in which you can

Figure 6.2. Digital microscope setup.

Figure 6.3. Image of a standard panel fabric at a magnification of 40X.

clearly see the warp and weft yarns in Figure 6.3. The distance between the warp yarns is 0.2 mm.

6.1 Test for Acoustical Transparency when Covering Loudspeakers and Sound Diffusors

To determine acoustical transparency of fabrics for use in covering loudspeakers, sound absorbers and diffusors, CAR has developed a process using the 6.3” square impedance tube, which has a frequency range of 63 Hz to 4,000 Hz. Two measurements are made; one determining the transparency of the fabric itself and another with the fabric applied to 2” of fiberglass. The test can be described with the help of Figure 6.4. Two measurement setups are shown. On the left, we show the speaker (at top), two of the four microphones, the fabric sample and a triangular anechoic termination. The anechoic termination has a gradually changing impedance and is intended to absorb all of the incident sound. The fabric under test will absorb, reflect back to the mic and transmit sound. All sound transmitted will be absorbed by the anechoic termination. Hence, a fully transparent fabric will appear to be 100 % absorptive. Thus we can use the absorption coefficient of the fabric only test as a measure of transparency. 100% absorption will be equivalent to 100% transparency, since no sound is reflected back to the mic. On the right side of Fig. 6.4 we show a setup with the fabric applied to 2” of fiberglass with a rigid termination. This measurement is used to determine how the fabric application affects the absorption of the core fiberglass. In Fig. 6.5, we show how these two measurements, along with the measurement of the 2” core fiberglas sample are interpreted. Anechoic termination transparency is shown at the top of each panel from 95% to 50%. The Transparency is expressed as the NRC of the fabric measured in front of an anechoic termination. The solid black line in all of the panels is the absorption of the core 2” fiberglas backing. The light gray areas show the spread in absorption (standard deviation from the mean) of all the fabrics with similar transparencies when applied to the 2” fiberglas core.

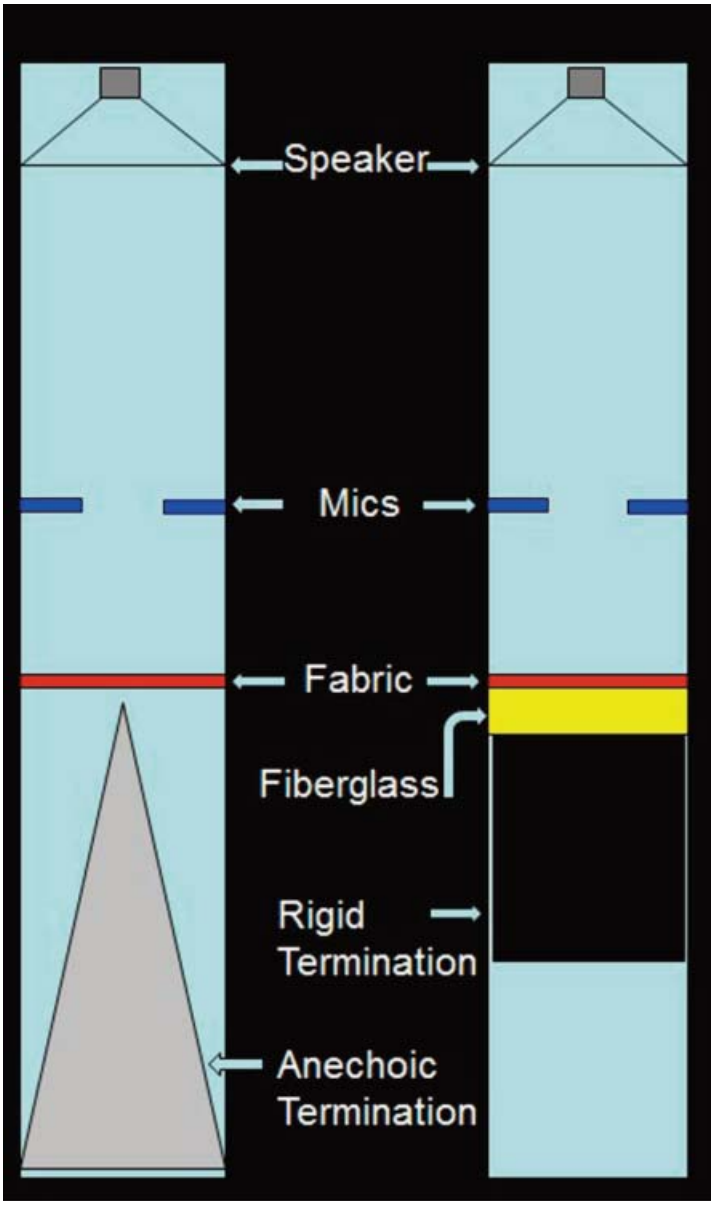

Figure 6.4. Fabric transparency measurement setup.

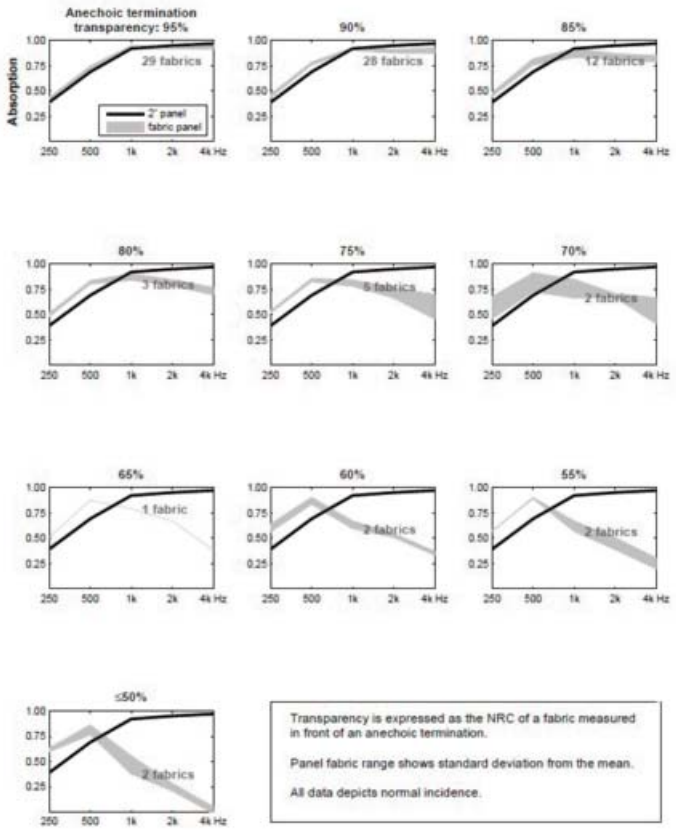

Figure 6.5. Anechoic termination transparency is shown at the top of each panel from 95% to 50%. The Transparency is expressed as the NRC of the fabric measured in front of an anechoic termination. The solid black line if the absorption of the core 2" fiberglas backing. The light gray areas show the range of absorption with the fabric applied to the 2" fiberglas core.

A very interesting observation can be made from these data. The term acoustical fabric traditionally described a textile that was transparent to incident sound so that it would not modify the absorption efficiency of the porous absorber core that it was used to cover. The fabrics with high transparencies will fall into this category. However, the testing indicates that it is possible to also constructively use fabrics backed with acrylics or other backing material and densly woven fabrics. The data show that as the transparency decreases, the high frequency absorption decreases, however, the low frequency absorption increases. If a design required a frequency balanced absorption, rather than the predominately high frequency absorption of fiberglas, a 75% transparent fabric might make a good choice as a sonic equalizers.

The report shown in Figure 6.6 is a summary of this testing.

Fabric transparency and panel absorption test

May 28 2013

For: RPG Diffusor Systems, Inc.
651-C Commerce Drive
Upper Marlboro MD 20774

Test sample: Fabric Under Test

Test method: The test method conforms to international standard ISO 10534-2 for determination of sound absorption coefficient and impedance in impedance tubes using the transfer-function method.

Transparency is expressed as absorption of fabric measured in front of an anechoic termination, and averaged from 250 to 2k Hz.

Transparency

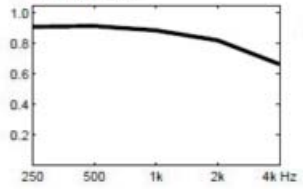

f [Hz]	%
250	91
500	91
1k	88
2k	82
4k	66
Ave	90

2" panel absorption

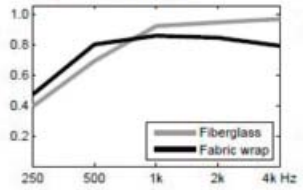

f [Hz]	%	%
250	39	47
500	69	80
1k	92	86
2k	95	84
4k	97	79
NRC	75	75

Peter D'Antonio, President | CEO

Chesapeake Acoustic Research Institute
651-C Commerce Drive Upper Marlboro MD 20774 United States
t +1 301 249 0044
f +1 301 390 3602

Figure 6.6. Fabric transparency report.

7 SCALE MODEL FABRICATION

While absorption testing is typically carried out at full scale, the testing of scattering samples can be carried out on scale models or at full scale. To quickly fabricate scale models, we utilize a 3D rapid prototyping printer, shown in Figure 7.1. The desired shape is created in 3D in AutoCAD and processed through the printer software, which slices

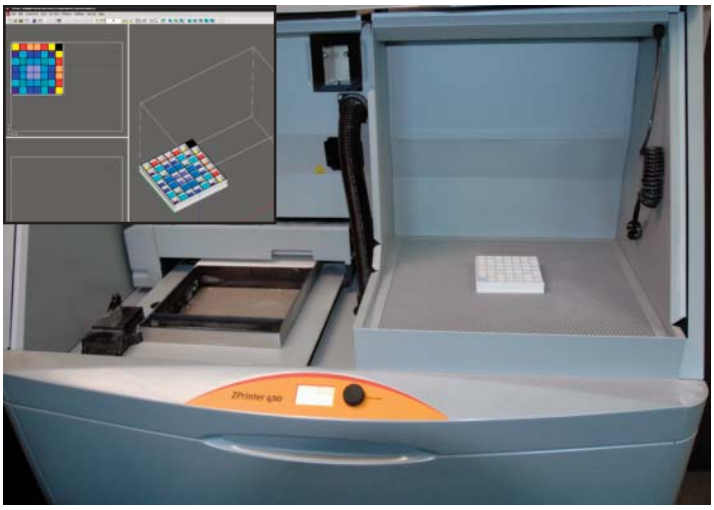

Figure 7.1. 3D Rapid Prototyping Printer with sample in the cleaning chamber and software screen upper

the shape into thin horizontal planes. The printer deposits a resin with a rasterizing printhead on each plane in turn, wherever there is material and the shape is built up vertically.

Figure 7.2. 1:5 scale model diffusors. Upper left: square based pyramid; Upper right: Modffusor; Lower left: Skyline; Lower right: Omniffusor. Coin in foreground is a US quarter.

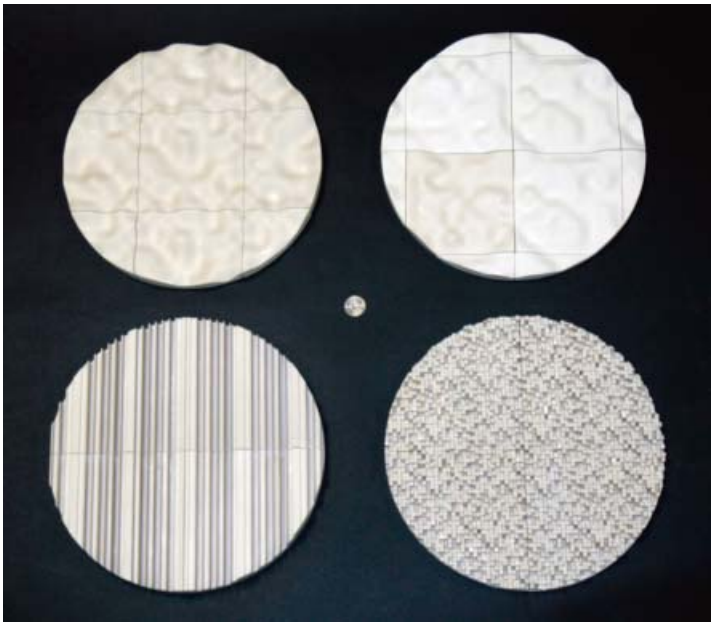

Figure 7.3. Four 1:10 scale samples for scattering coefficient testing according to ISO 17497-1. Upper left: Bicubic 8" deep; Upper right: Bicubic 4" deep; Lower left: Modffusor; Lower right: Skyline.

Figure 7.2 includes several 1:5 scale model diffusors fabricated for diffusion coefficient goniometer testing.

Figure 7.3 illustrates several 1:10 scale diffusor samples prepared for testing the scattering coefficient for potential use in a concert hall.

When larger samples are required, these can be fabricated in particleboard using a CNC router. An example of a 1:1.5 Skyline tested according to ISO 17497-1 is shown in Figure 7.4.

Figure 7.4. 1:1.5 sealed particle board Skylines on the rotating scattering coefficient table in the rev room for scattering coefficient testing.

8 SHAPE OPTIMIZATION SOFTWARE

An enduring characteristic of classic architecture is the beautiful statuary, relief ornamentation, columns and coffered ceilings. These beautiful features, coincidentally also provided useful sound scattering and excellent acoustics. This is evident in three of the renowned concert halls, namely the Concertgebouw in Amsterdam, the Musikvereinsaal in Vienna and Boston Symphony. Typically modern architecture lacks this intricate detailing and has evolved through a rectilinear era and is currently in a curvilinear or amorphous era. The acoustic fallout of these missing scattering elements is that modern rooms do not have good sound diffusion. What is needed are surfaces that complement contemporary architecture, the way that ornamentation complemented classic architecture.

Figure 8.1. Musikvereinsaal concert hall showing various forms or ornamentation leading to good sound diffusion.

Most readers will be familiar with aurally disfunctional rooms, like shopping malls or airports, where you can't understand announcements or school auditoriums and some performance venues, where music sounds terrible. Properly designed rooms need acoustic treatments on the walls, floor and ceiling to make speech intelligible and music beautiful.

In order to generate these modern sound diffusing surfaces, a software program called the Shape Optimizer was developed. The goal is essentially reverse engineering. Many acoustical products are created as a form follows function and architects have to find a way to integrate them into their designs. The Shape Optimizer allows the architect to propose a shape motif, e.g. a sinusoidal surface. Then this surface is mathematically described and the program evaluates, in an iterative manner, the thousands or more possible perturbations of this shape, which provide the desired sound scattering, so the architect gets the visual aesthetic they desire, while the acoustic consultant gets the best possible sonic performance.

To accomplish this, three things are needed, as shown in Figure 8.3. An accurate prediction method, a metric to evaluate performance and an intelligent search engine, which can quickly and efficiently navigate through the myriad shape possibilities. The prediction method utilized is a very accurate Boundary Element Method; the performance is monitored with a recently standardized metric called the diffusion coefficient, which characterizes how uniformly sound is scattered; and the intelligent search engine can be either a downhill simplex, which if you were in a mountain range quickly finds the lowest valley, or a genetic algorithm, which is similar to human genetics in which the fittest shape survives. Since current architecture is leaning towards curvilinear forms, we will present three examples,

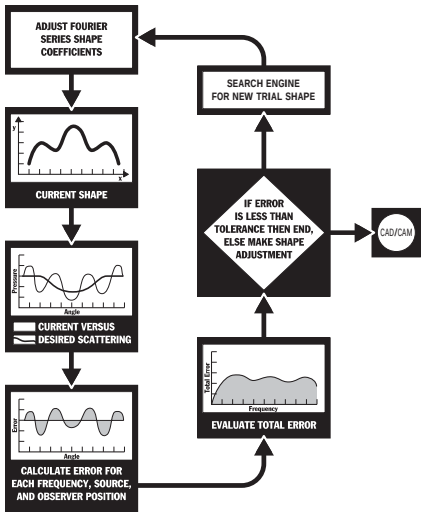

Figure 8.2. Shape Optimization software.

which were treated with this type of shape.

The first is a commercial theater called Cinerama in Seattle. The architect wanted an outer-worldly undulating ceiling for this state-of-the-art digital projection cinema. The final design and installation is shown in Figure 8.4. The architect was Boora Architects, Portland, OR and the acoustician was Harris-Grant Associates, Guilford, UK.

The second example involves a performance hall at the College of St. Rose, Albany, NY in which the architect and acoustician requested curved wood shapes on both the walls and ceiling. This can be seen in Figure 8.5. The architect was Saratoga Architects, Saratoga Springs, NY and the acoustician was AVL Designs, Penfield, NY.

A third example is the Thomas Deacon Academy in Peterborough, UK, shown in Figure 8.6. This is a very modern Sir Norman Foster design as can be seen from the exterior of the building, shown in the center of the photo collage. The Shape Optimizer was used to determine a curvilinear ceiling shape, shown upper left and right, as well as an amplitude modulated rear wall in the Lecture Hall, which mitigated the focusing effect of the concave rear wall. These shapes were intended to mimic the curvilinear shape of the building's exterior. The acoustician was Harris-Grant Associates, Guilford, UK.

Need To Predict Scattered Sound

BEM predictions with the Helmholtz-Kirchhoff equation were verified against numerous experimental measurements as being extremely accurate

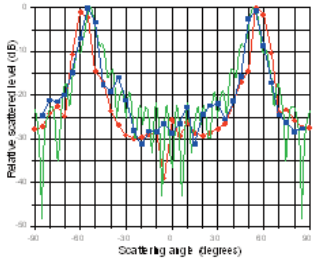

$$\alpha P(R) = P_s(Q,R) + \sum_q (P(q)\frac{\partial G(R,q)}{\partial n(q)} - G(R,q)\frac{\partial P(q)}{\partial n(q)})\Delta S_q$$

Need A Metric To Evaluate The Merit of a Surface Shape

The Diffusion Coefficient as described in AES-4id-2001 proved to be an effective metric for uniform scattering

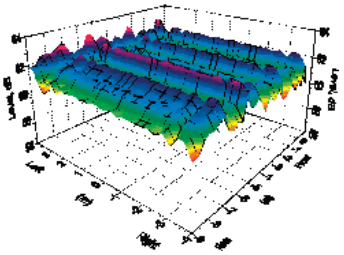

Need an Intelligent Search Engine To Navigate All Shapes

There are many robust search engines, we use the downhill simplex or genetic algorithm. Analogous to finding the lowest elevation in a mountainous terrain

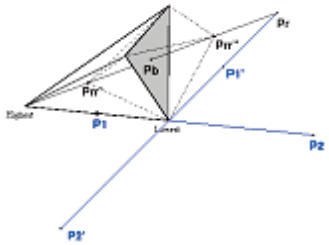

Figure 8.3. Three optimization techniques utilized in the Shape Optimizer.

This optimization approach, along with a thorough treatment of all that is currently known about sound absorbing and sound diffusing surfaces is presented in a reference text by the authors entitled “Acoustic Absorbers and Diffusers: Theory, Design and Application, 2n Edition, Taylor & Francis 2009”.

Figure 8.4. Optimized ceiling at Cinerama in Seattle, WA. The optimized ceiling provided an outer-worldly shape with fiber optic lighting to enhance the digital projection sound.

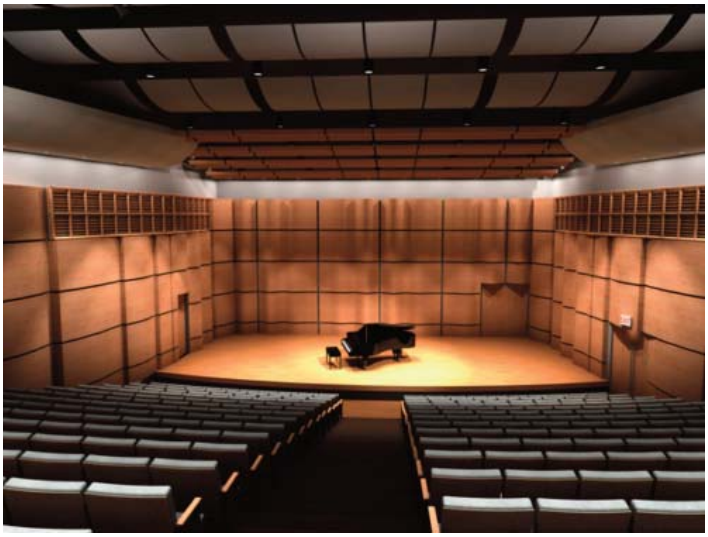

Figure 8.5. Optimized curvilinear wooden shapes on the walls and ceiling of the College of St. Rose, Massry Arts Center, Albany, NY. Rendering by Saratoga Architects.

Figure 8.6. Collage of images at the Thomas Deacon Academy in Peterborough, UK. Upper left and right: Ceiling mounted optimized spline in glass reinforced gypsum; Center: Outside photo: Lower left: Lecture hall optimized wavy rear wall; Lower right: Close up of the optimized wavy wall to minimize focusing effects.

9 CONCLUSION

Round robin measurements of the random incidence absorption coefficient have shown that the current standards result in a lack of accuracy and reproducibility among labs. Research is underway to improve accuracy by replacing traditional hanging diffusors with boundary mounted diffusors, to allow proper determination of the rev room's surface area and volume, evaluating edge diffraction and replacing the Sabine equation with that of Eyring. Calibration methods using an absorptive or reflective reference are also being evaluated to improve reproducibility. This author favors the use of a reflective or "low absorption" reference as discussed, since it is currently being used in ISO 179497-1 and ISO 17497-2 and reproducibility is found to be quite good at various scales. For example, in ISO 17497-1, the absorption attributed to the stationary and rotating table without sample is used to calibrate as and aspec, by measuring reverberation times T1 and T3, respectively, as shown in Figure 4.2 and Table 4.1. In ISO 17497-2, a reference reflector is used to remove the contribution from edge diffraction, as described in Section 5.1, Eq. (3).

The absorption coefficient according to ISO 354 and the scattering coefficient according to ISO 17497-1 are random incidence values, by virtue of their measurement. To determine a "random incidence" diffusion coefficient, one can simply average the directional coefficients. As an example, we provide a summary of directional and random incidence coefficients. We also introduce a "directional" absorption coefficient, which is becoming more and more relevant in acoustical design. This directional absorption coefficient is measured at the specular angle and is determined from a comparison between the directional specular scattering of a flat reference reflector and the sample. Because a diffusor primarily scatters sound, the word absorption is replaced by attenuation. A diffusor attenuates sound in a given direction, because the sound is uniformly scattered into many directions. We express this attenuation as excess specular attenuation compared to a reference reflector, by subtracting the spectrum of the diffusor from the reference response. Thus, the Excess Specular Attenuation is referenced to 0 dB, at which point the diffusor and sample responses are equal.

In Figure 9.1, we illustrate the directional incidence Diffusion Coefficients, Correlation Scattering Coefficients, Specular Zone Scattering Coefficients and the Excess Specular Attenuation at -30, -60, 0, 30 and 60 degrees, along with the tabulated data, for a Modffusor. In Figure 9.2, we illustrate the random incidence Diffusion, Scattering (either ISO, Correlation or Specular Zone) and Absorption coefficients, along with the tabulated data and a photo of the sample, which is suggested to completely characterize acoustical materials.

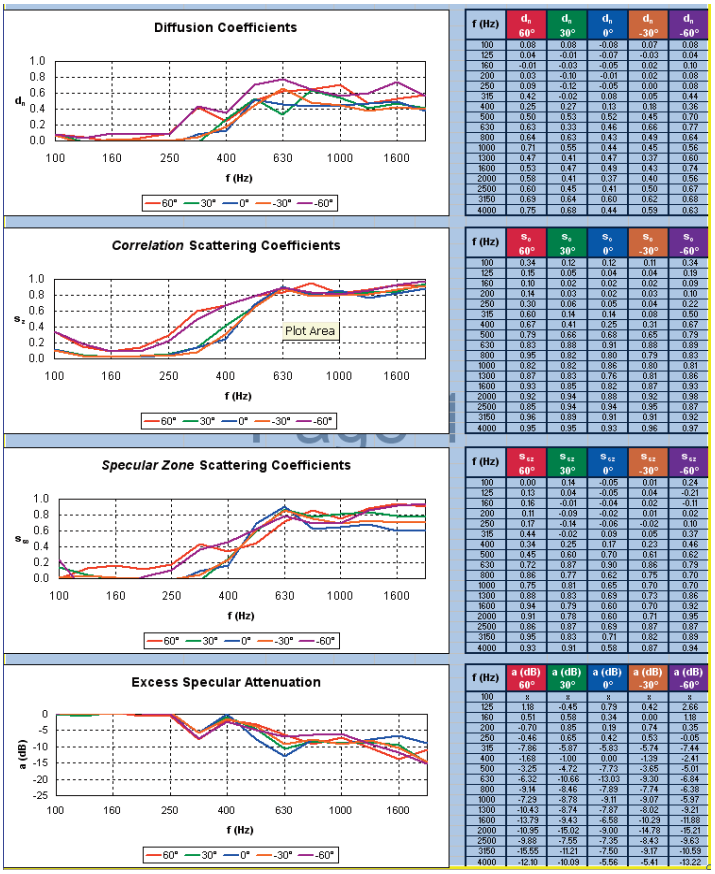

f (Hz)	d_s 60°	d_s 30°	d_h 0°	d_s -30°	d_s -60°
100	0.08	0.08	-0.08	0.07	0.08
125	0.04	-0.01	-0.07	-0.03	0.04
160	-0.01	-0.03	-0.05	0.02	0.10
200	0.03	-0.10	-0.01	0.02	0.08
250	0.09	-0.12	-0.05	0.00	0.08
315	0.42	-0.02	0.08	0.05	0.44
400	0.25	0.27	0.13	0.18	0.36
500	0.50	0.53	0.52	0.45	0.70
630	0.63	0.33	0.46	0.66	0.77
800	0.64	0.63	0.43	0.49	0.64
1000	0.71	0.55	0.44	0.45	0.56
1300	0.47	0.41	0.47	0.37	0.60
1600	0.53	0.47	0.49	0.43	0.74
2000	0.58	0.41	0.37	0.40	0.56
2500	0.60	0.45	0.41	0.50	0.67
3150	0.69	0.64	0.60	0.62	0.68
4000	0.75	0.68	0.44	0.59	0.63

f (Hz)	s_c 60°	s_c 30°	s_c 0°	s_c -30°	s_c -60°
100	0.34	0.12	0.12	0.11	0.34
125	0.15	0.05	0.04	0.04	0.19
160	0.10	0.02	0.02	0.02	0.09
200	0.14	0.03	0.02	0.03	0.10
250	0.30	0.06	0.05	0.04	0.22
315	0.60	0.14	0.14	0.09	0.50
400	0.67	0.41	0.25	0.31	0.67
500	0.79	0.66	0.68	0.65	0.79
630	0.83	0.88	0.91	0.88	0.89
800	0.95	0.82	0.90	0.79	0.83
1000	0.82	0.82	0.86	0.80	0.81
1300	0.87	0.83	0.76	0.81	0.86
1600	0.93	0.85	0.82	0.87	0.93
2000	0.92	0.94	0.88	0.92	0.98
2500	0.85	0.94	0.94	0.95	0.87
3150	0.96	0.89	0.91	0.91	0.92
4000	0.95	0.95	0.93	0.96	0.97

f (Hz)	s_{c2} 60°	s_{c2} 30°	s_{c2} 0°	s_{c2} -30°	s_{c2} -60°
100	0.00	0.14	-0.05	0.01	0.24
125	0.13	0.04	-0.05	0.04	-0.21
160	0.16	-0.01	-0.04	0.02	-0.11
200	0.11	-0.09	-0.02	0.01	0.02
250	0.17	-0.14	-0.06	0.02	0.10
315	0.44	-0.02	0.09	0.05	0.37
400	0.34	0.25	0.17	0.23	0.46
500	0.45	0.60	0.70	0.61	0.62
630	0.72	0.87	0.90	0.86	0.79
800	0.86	0.77	0.62	0.75	0.70
1000	0.75	0.91	0.65	0.70	0.70
1300	0.88	0.83	0.63	0.73	0.86
1600	0.94	0.79	0.60	0.70	0.92
2000	0.91	0.78	0.60	0.71	0.95
2500	0.86	0.87	0.63	0.87	0.87
3150	0.95	0.83	0.71	0.82	0.89
4000	0.93	0.91	0.58	0.87	0.94

f (Hz)	a (dB) 60°	a (dB) 30°	a (dB) 0°	a (dB) -30°	a (dB) -60°
100	x	x	x	x	x
125	1.18	-0.45	0.79	0.42	2.66
160	0.51	0.58	0.34	0.00	1.18
200	-0.70	0.85	0.19	0.74	0.35
250	-0.46	0.85	0.42	0.53	-0.05
315	-7.86	-5.87	-5.83	-5.74	-7.44
400	-1.68	-1.00	0.00	-1.39	-2.41
500	-3.25	-4.72	-7.73	-3.65	-5.01
630	-6.32	-10.66	-13.03	-9.30	-6.84
800	-9.14	-9.46	-7.89	-7.74	-6.38
1000	-7.29	-8.78	-9.11	-9.07	-5.97
1300	-10.43	-8.74	-7.87	-8.02	-9.21
1600	-13.79	-9.43	-6.58	-10.29	-11.88
2000	-10.95	-15.02	-9.00	-14.79	-15.21
2500	-9.88	-7.55	-7.35	-8.43	-9.63
3150	-16.55	-11.21	-7.50	-9.17	-10.59
4000	-12.10	-10.09	-5.56	-5.41	-13.22

Figure 9.1. Directional Incidence Coefficients for the Modffusor.

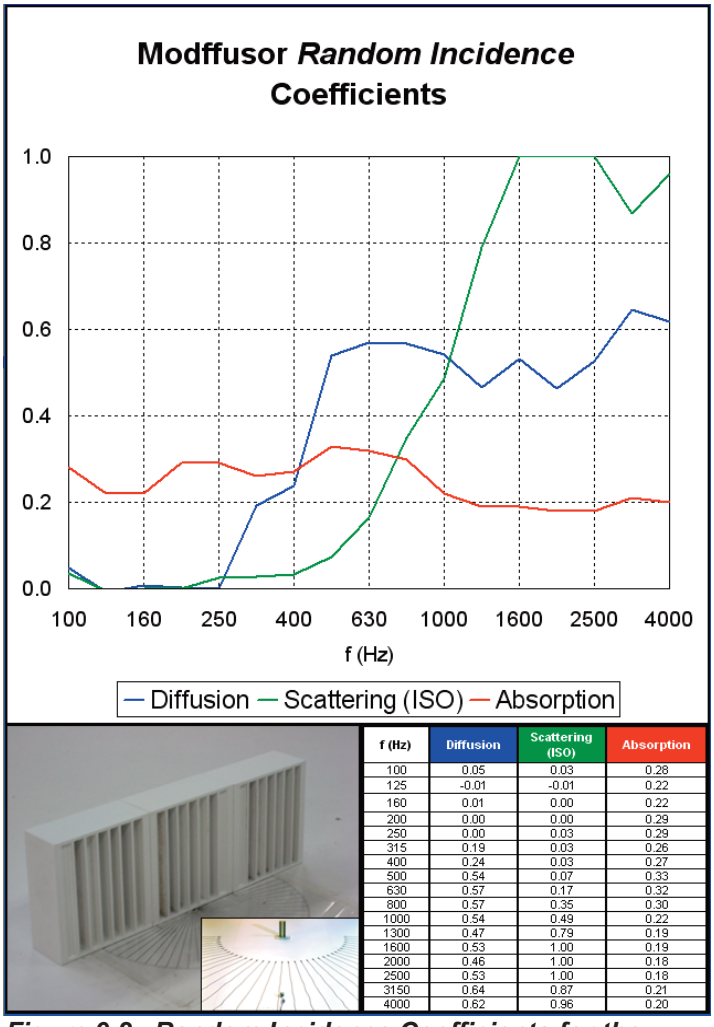

f (Hz)	Diffusion	Scattering (ISO)	Absorption
100	0.05	0.03	0.28
125	-0.01	-0.01	0.22
160	0.01	0.00	0.22
200	0.00	0.00	0.29
250	0.00	0.03	0.29
315	0.19	0.03	0.26
400	0.24	0.03	0.27
500	0.54	0.07	0.33
630	0.57	0.17	0.32
800	0.57	0.35	0.30
1000	0.54	0.49	0.22
1300	0.47	0.79	0.19
1600	0.53	1.00	0.19
2000	0.46	1.00	0.18
2500	0.53	1.00	0.18
3150	0.64	0.87	0.21
4000	0.62	0.96	0.20

Figure 9.2. Random Incidence Coefficients for the Modffusor, along with tabulated data and a photo of the sample.